



UNIVERSITÀ DI PARMA

ARCHIVIO DELLA RICERCA

University of Parma Research Repository

Highly siderophile and chalcophile element behaviour in abyssal-type and supra-subduction zone mantle: new insights from the New Caledonia ophiolite

This is the peer reviewed version of the following article:

Original

Highly siderophile and chalcophile element behaviour in abyssal-type and supra-subduction zone mantle: new insights from the New Caledonia ophiolite / Secchiari, Arianna; Gleissner, Philipp; Li, Chunhui; Goncharov, Alexey; Becker, Harry; Bosch, Delphine; Montanini, Alessandra. - In: LITHOS. - ISSN 0024-4937. - 354-355:(2020), pp. 105338.1-105338.17. [10.1016/j.lithos.2019.105338]

Availability:

This version is available at: 11381/2868206 since: 2024-12-24T07:53:09Z

Publisher:

Elsevier B.V.

Published

DOI:10.1016/j.lithos.2019.105338

Terms of use:

Anyone can freely access the full text of works made available as "Open Access". Works made available

Publisher copyright

note finali coverpage

(Article begins on next page)

02 May 2026

Manuscript Number:

Title: Highly siderophile and chalcophile element behaviour in abyssal-type and supra-subduction zone mantle: new insights from the New Caledonia ophiolite

Article Type: VSI:EMAW- Mantle Paradigms

Keywords: Re-Os geochemistry
Highly siderophile elements
New Caledonia ophiolite
Sub-arc mantle
Depleted mantle sections

Corresponding Author: Dr. Arianna Secchiari, PhD

Corresponding Author's Institution: University of Parma

First Author: Arianna Secchiari, PhD

Order of Authors: Arianna Secchiari, PhD; Philipp Gleissner, PhD; Chunhui Li, PhD; Alexey Goncharov, PhD; Harry Becker, Professor; Alessandra Montanini, PhD; Delphine Bosch, PhD

Abstract: The New Caledonia Ophiolite hosts one of the largest obducted mantle sections worldwide, offering a unique opportunity to investigate key mantle processes. The ophiolite comprises refractory harzburgites, locally overlain by mafic-ultramafic cumulates, and minor lherzolites. Previous geochemical studies indicated that the lherzolites are akin to abyssal-type peridotites, while the harzburgites underwent multiple melting episodes in MOR and supra-subduction zone environments, followed by late stage metasomatism.

In this work, Os isotopes, highly siderophile (HSE) and chalcophile element data are reported for the New Caledonia peridotites, in order to constrain the behaviour of these elements in abyssal-type and fore-arc mantle.

The variably serpentinised lherzolites (LOI = 6.4 - 10.7 %) yield slightly subchondritic to suprachondritic initial Os isotopic compositions ($^{187}\text{Os}/^{188}\text{Os}_i = 0.1273\text{-}0.1329$) and subchondritic to chondritic Re/Os ratios (0.04-0.11). The gently sloping HSE patterns with increasing depletion towards Au show concentrations in the range of other lherzolites from MOR or continental setting. Sulphur contents are high and variable (202-1268 ppm), and were likely increased during serpentinisation. By contrast, Se/Te ratios and concentrations are within the range of primitive mantle (PM) values, meaning that these elements were not significantly mobilised during serpentinisation.

Despite displaying homogenous petrographic and geochemical features, the harzburgites are characterised by extremely heterogeneous Re-Os and HSE compositions.

Type-A harzburgites exhibit subchondritic $^{187}\text{Os}/^{188}\text{Os}_i$ (0.1203-0.1266) and low Re/Os ratios (0.01-0.04). The strong IPGE-PPGE fractionations ($\text{PdN}/\text{IrN} = 0.21\text{-}0.56$) coupled with positive Pt anomalies and S-Se-Te abundances often below the detection limit suggest high melt extraction

rates, resulting in sulphide consumption and Os-Ru metal alloy stabilisation.

Type-B harzburgites possess strongly fractionated, Os-Ir-Pt poor (Os = 0.003-0.072 ng/g, Ir = 0.0015-0.079 ng/g) and Pd-Re enriched patterns, associated with chondritic to suprachondritic measured $^{187}\text{Os}/^{188}\text{Os}$ (0.127-0.153). These characters are uncommon for highly depleted mantle residues. Interaction with an oxidised component does not appear as a viable mechanism to account for the IPGE-depleted patterns of type-B harzburgites, as calculated oxygen fugacities are close to the FMQ buffer ($\text{Log } \Delta\text{FMQ} = 0.20$ to 0.48). The lower $f\text{O}_2$ conditions register by type-B harzburgites compared to type-A likely records $f\text{O}_2$ lowering due to continued melt extraction at un-buffered $f\text{O}_2$ conditions. Type-B patterns may thus derive from slightly higher melting degrees, finally leading to Os-Ir-Pt release into the silicate melt. We propose that HSE geochemistry of the New Caledonia peridotites reveals superimposition of geochemical characters related to the recent Eocene evolution on a mantle source bearing a long term (> 1 Ga) evolution.

Abstract

The New Caledonia Ophiolite hosts one of the largest obducted mantle sections worldwide, offering a unique opportunity to investigate key mantle processes. The ophiolite comprises refractory harzburgites, locally overlain by mafic-ultramafic cumulates, and minor lherzolites. Previous geochemical studies indicated that the lherzolites are akin to abyssal-type peridotites, while the harzburgites underwent multiple melting episodes in MOR and supra-subduction zone environments, followed by late stage metasomatism.

In this work, Os isotopes, highly siderophile (HSE) and chalcophile element data are reported for the New Caledonia peridotites, in order to constrain the behaviour of these elements in abyssal-type and fore-arc mantle.

The variably serpentinised lherzolites (LOI = 6.4 - 10.7 %) yield slightly subchondritic to suprachondritic initial Os isotopic compositions ($^{187}\text{Os}/^{188}\text{Os}_i = 0.1273\text{-}0.1329$) and subchondritic to chondritic Re/Os ratios (0.04-0.11). The gently sloping HSE patterns with increasing depletion towards Au show concentrations in the range of other lherzolites from MOR or continental setting. Sulphur contents are high and variable (202-1268 ppm), and were likely increased during serpentinisation. By contrast, Se/Te ratios and concentrations are within the range of primitive mantle (PM) values, meaning that these elements were not significantly mobilised during serpentinisation. Despite displaying homogenous petrographic and geochemical features, the harzburgites are characterised by extremely heterogeneous Re-Os and HSE compositions.

Type-A harzburgites exhibit subchondritic $^{187}\text{Os}/^{188}\text{Os}_i$ (0.1203-0.1266) and low Re/Os ratios (0.01-0.04). The strong IPGE-PPGE fractionations ($\text{Pd}_N/\text{Ir}_N = 0.21\text{-}0.56$) coupled with positive Pt anomalies and S-Se-Te abundances often below the detection limit

suggest high melt extraction rates, resulting in sulphide consumption and Os-Ru metal alloy stabilisation.

Type-B harzburgites possess strongly fractionated, Os-Ir-Pt poor (Os = 0.003-0.072 ng/g, Ir = 0.0015-0.079 ng/g) and Pd-Re enriched patterns, associated with chondritic to suprachondritic measured $^{187}\text{Os}/^{188}\text{Os}$ (0.127-0.153). These characters are uncommon for highly depleted mantle residues. Interaction with an oxidised component does not appear as a viable mechanism to account for the IPGE-depleted patterns of type-B harzburgites, as calculated oxygen fugacities are close to the FMQ buffer (Log ΔFMQ = 0.20 to 0.48). The lower f_{O_2} conditions register by type-B harzburgites compared to type-A likely records f_{O_2} lowering due to continued melt extraction at un-buffered f_{O_2} conditions. Type-B patterns may thus derive from slightly higher melting degrees, finally leading to Os-Ir-Pt release into the silicate melt. We propose that HSE geochemistry of the New Caledonia peridotites reveals superimposition of geochemical characters related to the recent Eocene evolution on a mantle source bearing a long term (> 1 Ga) evolution.

A comprehensive Re-Os, highly siderophile and chalcophile element investigation of the New Caledonia peridotites is presented.

HSE patterns of the lherzolites reflect low partial melting degrees of a mantle source that previously experienced melt percolation and radiogenic Os ingrowth.

Based on HSE and Os isotopic signature, two big groups of harzburgites (*type-A and B*) can be identified.

HSE and Re-Os systematics of type-A harzburgites are consistent with high melt extraction degrees, resulting in sulphide exhaustion and Os-Ru metal alloys stabilisation.

The HSE and Re-Os features of type-B harzburgites may record higher partial melting degrees and Os-Ir-Pt release into silicate melt after continued melt extraction.

1

2 1. Introduction

3

4 Highly siderophile elements (HSE: PGE+ Au-Re) are powerful geochemical tracers that
5 can provide useful information for a variety of mantle processes, such as mantle
6 melting, metasomatism and melt-fluid/mantle interaction (e.g. Luguet et al., 2001,
7 2003, 2007; Lorand et al., 2008; Ackerman et al., 2009). However, our knowledge
8 concerning the behaviour of HSE in mantle source rocks of primitive arc magmas and
9 the role of the subduction zone environment on HSE partitioning (i.e. hydrous melting,
10 melt/fluid-mantle interaction) still remains quite fragmentary. Furthermore, although
11 abundant HSE data are now available for different types of mantle peridotites, HSE
12 data on fore-arc peridotites are remarkably scarce (e.g. Becker and Dale, 2016).

13 The New Caledonia ophiolite (Peridotite Nappe) hosts one of the largest and best
14 preserved mantle sections worldwide, providing an excellent opportunity to
15 investigate upper mantle processes. The rock exposures are dominated by harzburgite
16 tectonites bearing a supra-subduction zone affinity (Marchesi et al., 2009; Ulrich et
17 al., 2010; Pirard et al., 2013; Secchiari et al., 2019a). The main geochemical and
18 isotopic features of these rock-types reflect a complex polyphase evolution, including
19 several melting episodes in different geodynamic settings and subduction zone
20 metasomatism (Marchesi et al., 2009; Ulrich et al., 2010; Secchiari et al., 2019a).
21 Minor abyssal-type spinel and plagioclase lherzolites, with compositions similar to
22 abyssal peridotites, occur as discrete bodies in the north-western part of the island.
23 The lherzolites record a different history compared to the extremely refractory
24 harzburgites, as highlighted by their different geochemical signature (Ulrich et al.,
25 2010; Secchiari et al., 2016).

26 In this work, a set of fully characterised peridotites (i.e. whole rock and in situ major
27 and trace element contents, Sr-Nd-Pb isotopes) from New Caledonia (Secchiari et al.,
28 2016, 2019a) has been used to investigate Re-Os, HSE and chalcophile element (S-
29 Se-Te) systematics. The main aims of this work are: 1) to examine the behaviour of
30 these elements in the lherzolites (i.e. presumed abyssal peridotites) and in the ultra-
31 depleted harzburgites, which may represent rocks from a former supra-subduction
32 zone mantle wedge; 2) to constrain the behaviour of HSE and chalcophile elements
33 during subduction zone processes.

34

35 2. Geological setting and petrological background

36

37 New Caledonia is a NW–SE elongated island located in the SW Pacific region, between
38 the eastern margin of Australia and the Vanuatu archipelago (Fig. 1a). The island
39 represents the emerged portion of the submarine Norfolk Ridge and it is composed by
40 a mosaic of volcanic, sedimentary and metamorphic terranes, ranging in age from
41 Permian to Miocene (Aitchison et al., 1995; Cluzel et al., 2001, 2012; Lagabrielle et
42 al., 2013). These terranes were amalgamated during two major tectonic events: 1) an
43 Early Cretaceous tectonic convergence phase (Paris, 1981) and 2) a Paleocene to Late
44 Eocene subduction culminated in the obduction of the ophiolite. Both events were
45 characterized by high-pressure low-temperature (HP-LT) metamorphism in connection
46 with plate convergence. New Caledonia can be sub-divided into four main geological
47 domains (Cluzel et al., 2001; see Fig. 1): (i) the Basement units (pre-Late Cretaceous
48 basement and Late Coniacian-to-Late Eocene sedimentary cover), (ii) the Cenozoic
49 HP-LT metamorphic belt, (iii) the basaltic Poya Terrane and (iv) a large slab of
50 peridotites, i.e. the Peridotite Nappe.

51 The Peridotite Nappe represents an allochthonous sheet of oceanic lithosphere
52 belonging to the former South Loyalty basin thrust on the continental basement of the
53 Norfolk Ridge at the end of the Eocene subduction. The emplacement of the ophiolitic
54 nappe resulted from the failed subduction of the Norfolk Ridge tip in a NE-dipping
55 subduction zone, which culminated in the obduction of the Loyalty subarc lithosphere
56 ~ 34 Ma ago (Cluzel et al. 2012).

57 The Peridotite Nappe has an extension of about 8000 km² and is mostly exposed in
58 the Massif du Sud, where a thick harzburgite–dunite unit, locally overlain by
59 kilometre-scale lenses of mafic and ultramafic intrusives, crops out. The sequence is
60 believed to represent a crust-mantle boundary that records the onset of Eocene
61 subduction in a nascent arc setting (Marchesi et al., 2009; Pirard et al., 2013;
62 Secchiari et al., 2018). Recent geochemical studies have shown that the ultramafic
63 intrusives (i.e. dunites and wehrlites) crystallised from variably depleted melts with
64 island arc basalt affinity, after massive interactions with the underlying harzburgite
65 (Marchesi et al., 2009; Pirard et al., 2013). In contrast, the mafic rocks (i.e.
66 gabbro-norites) rather have a cumulate origin (Marchesi et al., 2009; Pirard et al.,
67 2013; Secchiari et al., 2018) and derive from crystallization of primitive, non-
68 aggregated, ultra-depleted melts showing involvement of a subduction-related
69 component in their source (Secchiari et al., 2018).

70 The harzburgites are also exposed in the northern Tiébaghi massif (Ulrich et al., 2010)
71 or as sparse tectonic klippen in the central part of the island (e.g. Kopeto, Poya,
72 Koniambo), where exceptionally fresh peridotites display primary mineral assemblages
73 similar to the more serpentinitised rocks of the Massif du Sud.

74 The New Caledonia harzburgites bear an overall ultra-depleted composition, inherited
75 from a complex multistage evolution linked to the development of the Eocene
76 subduction system (Marchesi et al., 2009; Ulrich et al., 2010; Secchiari et al., 2019a).
77 Geochemical studies have proposed that the harzburgites formed by high degrees of

78 fluid-assisted melting (up to 20-25 % in a supra-subduction zone environment, see
79 Marchesi et al., 2009; Ulrich et al., 2010). More recently, the work of Secchiari et al.
80 (2019a) provided further constraints on the evolution of the harzburgites, tracking
81 their history from melting to late stage metasomatism. Accordingly, the harzburgites
82 underwent two partial melting episodes in the spinel stability field: a first melting
83 phase in a MOR setting (15% melting degrees), followed by hydrous melting in a
84 supra-subduction zone setting (up to 18% fluid-assisted melting). Post-melting
85 cooling and re-equilibration at lithospheric conditions was accompanied by interaction
86 with slab-derived hydrous melts bearing an ultra-depleted composition (Secchiari et
87 al., 2019a,b). These metasomatic processes in the harzburgites are indicated by the
88 widespread occurrence of secondary metasomatic phases (i.e. thin films of Al_2O_3 -,
89 CaO- poor orthopyroxene, and low Al_2O_3 and Na_2O clinopyroxene), L-MREE and Zr-Hf
90 bulk rock enrichments, as well as by the unradiogenic Nd isotopic ratios shown by
91 some samples (Secchiari et al., 2019a).

92 Compared to the harzburgites from the central and the southern massifs, Tiébaghi
93 samples display a more fertile nature, as indicated by higher trace element
94 concentrations as well as by the occurrence of a small fraction (up to 4 vol.%) of
95 clinopyroxene (see Ulrich et al., 2010; Secchiari, PhD thesis).

96 The main geochemical and petrological features of the spinel and plagioclase
97 lherzolites are thought to reflect moderate melting degrees (8-9%) in a MOR
98 environment, followed by refertilisation by depleted MORB-type melts, yielding
99 plagioclase lherzolites. The main petrological and geochemical features of these
100 lithotypes have been described in detail by Secchiari et al. (2016).

101

102 2.1 Sample description

103

104 In this contribution, seventeen samples of peridotites fully characterised for lithophile
105 element geochemistry (i.e. major, trace element and Sr-Nd-Pb isotope compositions)
106 were analysed for mass fractions of all PGE, Re, Au, S, Se and Te and $^{187}\text{Os}/^{188}\text{Os}$.
107 Detailed descriptions of the lherzolites and harzburgites, including trace element
108 chemistry and Sr-Nd-Pb isotopes, are provided in Secchiari et al. (2016) and Secchiari
109 et al. (2019a, b), respectively.

110 Lherzolite samples are from the Poum and Babouillat areas, while the harzburgites
111 were collected from several outcrops and mine zones along the island: Yat e, Kopeto,
112 Poya, Poro and Ti ebaghi (Fig. 1b and Table 1). The lherzolites include serpentinitised
113 (LOI= 6.9 - 10.7 %) spinel and plagioclase lherzolites, while the harzburgites are
114 typically not or only little serpentinitised (LOI = 0 - 3 %), except for samples YA1, TI1
115 and TI2 (LOI = 6.0 - 9.0 %).

116 Both lherzolites and harzburgites are low strain mantle tectonites, showing dominant
117 porphyroclastic textures (Fig. S1a-b) and local protomylonite development. Spinel
118 lherzolites have 7-8 vol.-% clinopyroxene and display a typical abyssal-type REE
119 signature. The plagioclase lherzolites show melt impregnation microstructures (Fig.
120 S1b) and are slightly enriched in incompatible trace element enrichments (REE, Ti, Y,
121 and Zr) with respect to the spinel lherzolites. Harzburgites are extremely depleted
122 rocks, as highlighted by the general absence of clinopyroxene (with the exception of
123 sample TI2, where clinopyroxene is ~ 4 vol. %, Fig. S1c) and the very low
124 incompatible trace element contents (Secchiari et al., 2019a). The primary mantle
125 paragenesis is composed of olivine, orthopyroxene and spinel. The occurrence of thin
126 films of metasomatic ortho- and clinopyroxene (Fig. S1d) was interpreted as the
127 result of percolation by small fractions of subduction-related magmas (Secchiari et al.,
128 2019a-b).

129 Rare sulphide grains with variable size, shape and position have been recognised in
130 the lherzolites and were analysed for their major element chemistry in samples BA1

131 and POU2 (see Table S1). Small (40 to 100 μm x 30 to 80 μm) sulphide inclusions
132 (Fig. S2a-e), bearing polyhedral or spherical shape, have been observed within olivine
133 and pyroxene porphyroclasts. Interstitial sulphide grains occur as polyhedral blebs
134 (Fig. S2f), up to 300 x 100/150 μm in maximum dimensions, and are generally
135 located at olivine-pyroxene grain boundaries. Sulphide composition is relatively
136 homogeneous (Table S1 and Fig. S2), with Ni-poor (Fe/Ni=1.4-2.5) monosulphide
137 solid solution (Guo et al., 1999) being the most abundant phase. Ni-rich (Fe/Ni =0.7-
138 0.8) pentlandite has also been identified in the sample POU2. The sulphides frequently
139 show lamellae and rims made by Fe-oxides/hydroxides due to desulphidation
140 reactions.

141 3. Analytical methods

142

143 3.1 HSE and chalcophile elements

144

145 Seven Iherzolites and ten harzburgites (including four duplicates) have been analysed
146 in the geochemistry laboratory at Freie Universität for HSE, S, Se, Te mass fractions
147 in whole rocks and $^{187}\text{Os}/^{188}\text{Os}$.

148 Detailed procedure descriptions have been given in previous work from this laboratory
149 (e.g. Fischer-Gödde et al., 2011; Wang et al., 2013; Wang and Becker, 2013). The
150 methods will only be briefly summarized below.

151 About 2.5 g of sample powder was weighed into 90 ml quartz glass digestion vessels
152 and spiked with mixed ^{191}Ir - ^{99}Ru - ^{194}Pt - ^{105}Pd , ^{77}Se - ^{125}Te , ^{185}Re - ^{190}Os and ^{34}S solutions.
153 Then, 5 ml 14 mol/L, N_2 -bubbled HNO_3 and 2.5 ml 9 mol/L HCl were added. The
154 vessels were immediately sealed with Teflon tape and samples were digested for 16 h
155 at 320°C and 100 bar. After digestion, osmium was extracted from the reverse aqua

156 regia into chloroform, back extracted into HBr (Cohen and Waters, 1996), and further
157 purified by micro distillation from a H₂SO₄-dichromate solution into 15 µl of HBr (Birck
158 et al., 1997)

159 Osmium isotopes were determined as OsO₃⁻ in negative mode using the Thermo
160 Finnigan Triton TIMS, using a secondary electron multiplier. Signal intensities of the
161 spike isotope ¹⁹⁰Os of samples were ~ 150,000–500,000 cps. Standard runs with
162 different amounts of Os on the filament (10 pg and 100 pg) were also run in between
163 the studied samples, yielding an average value of 0.1139 ± 0.0002 (2 s. d., n = 24)
164 for 100 pg loads. Two hundreds scans were collected in each measurement for high-
165 Os samples, while at least 120-140 scans were obtained for the low-Os samples. Raw
166 data were corrected for isobaric OsO₃⁻ interferences, mass fractionation using the
167 ¹⁹²Os/¹⁸⁸Os ratio of 3.08271, contributions from the Os spike solution and blank
168 contributions. ¹⁸⁷Os/¹⁸⁸Os were finally adjusted relative to the mean of the Os
169 standard. The oxygen isotope compositions used for the oxide correction of Os oxide
170 molecules were ¹⁸O/¹⁶O of 0.00204 and ¹⁷O/¹⁶O of 0.00037 (Nier, 1950).

171 About 50% of the digestion solution was used for separation of the HSE fraction and
172 about 30% for S–Se–Te separation. Chemical separation of the HSE fraction from the
173 matrix was performed on columns filled with 10 ml of pre-cleaned Eichrom 50W-X8
174 (100–200 mesh) cation exchange resin (Fischer-Gödde et al., 2011). During
175 separation, the HSE fraction was collected in 14 ml 0.5 mol/L HCl-40 vol.% acetone
176 mixture. After the volume of the solution has been reduced to about 2 ml it was
177 analysed for Au, Re, Ir and Pt. In order to remove interfering Cd, the remaining
178 solution was further purified in 0.2 mol/L HCl on 3 ml Eichrom 50W-X8 (100–200
179 mesh) resin. The collected solution was evaporated to near dryness and the residue
180 was taken up in 0.28 M HNO₃ for ICP-MS analysis. The analyses were carried out
181 using a single collector Element XR instrument. We used either a Scott-type spray

182 chamber (Re, Ir, Pt, Au) or an Aridus-I desolvator (Ir, Ru, Pt, Rh, Pd) at an oxide
183 formation rate of $\text{CeO}^+/\text{Ce}^+ < 0.004$.

184 A two-step ion exchange chromatography method was used for separation of S, Se
185 and Te (see Wang et al., 2013). Sulphur measurements were performed on the S-Se
186 fraction at medium mass resolution mode on the Element XR. Selenium and Te were
187 measured using a double pass Scott type glass spray chamber at low mass resolution
188 mode on the Element XR, combined with a hydride generation sample introduction
189 system by reacting the sample solution with 1 g/100 g NaBH_4 in 0.05 mol/L NaOH
190 (see Wang et al., 2013 for details).

191 For each batch of analysis, one procedural blank has been used. Procedural blanks
192 yielded the following mean values (± 1 s.d., $n = 4-5$): Re = 2.5 ± 2.0 pg; Os = $0.5 \pm$
193 0.3 pg with $^{187}\text{Os}/^{188}\text{Os}$ ratios of 0.14 ± 0.03 ; Ir = 15 ± 5 pg; Ru = 45 ± 14 pg; Rh =
194 24 ± 22 pg; Pt = 23 ± 29 pg; Pd = 640 ± 330 pg; Au = 4 ± 2 pg; Te = 1.1 ± 0.8 ng;
195 Se = 2.3 ± 0.8 ng; S = 2.8 ± 0.7 μg . Samples were corrected for total procedural
196 blanks using the mean values. Blank corrections for Re are negligible for most of the
197 analysed samples ($\leq 0.3 - 0.8$ %), but more significant for the harzburgites ($\sim 4 - 8$
198 %). Blank corrections for Pt and Pd are again negligible for the Iherzolites ($\sim 0.2 - 0.3$
199 %) a few percents for the harzburgites ($\sim 0.4 - 4$ %, with the exception of KPT2,
200 KPT5 and PO3 for which the correction for Pt is $\sim 11 - 36$ %). Blanks of Os, Ir, Ru and
201 Rh are insignificant for most of the samples (≤ 0.4 %) but higher for the most
202 depleted harzburgites, i.e. KPT2, KPT5 ($\sim 2 - 7$ % for Os, Ir, Rh) and PO3 (~ 9 % for
203 Os and Ir, 13 % for Rh). Blank corrections for S, Se and Te in Iherzolites range
204 between 1 - 1.7 % (S - Se) and 3-6% (Te), while for harzburgites blank corrections
205 for these elements strongly affected the obtained results (corrections $\sim 10 - 26$ % for
206 S and up to 40 - 80% for Se and Te), given the very low measured abundances.

207

208 3.2 Oxygen fugacity

209

210 Iron oxidation state in studied spinel was measured using flank approach designed for
211 the JEOL JXA-8200 electron microprobe analyser at Freie Universität on a collection of
212 natural and synthetic spinel standards characterized for their $\text{Fe}^{3+}/\Sigma\text{Fe}$ at IPGG RAS
213 (St. Petersburg) using Mössbauer spectroscopy (Goncharov, 2018). The analytical
214 procedure was similar to experiments performed over the last decades to study
215 $\text{Fe}^{3+}/\Sigma\text{Fe}$ in mantle garnets after procedure developed by (Höfer and Brey, 2007). The
216 flank positions were calculated from the difference spectrum of almandine-andradite
217 for the spectrometer in wavelength range related to $\text{FeL}\alpha$ and $\text{FeL}\beta$ lines. $\text{FeL}\alpha$ and
218 $\text{FeL}\beta$ intensities were collected at a wavelength of flank lines for 300 seconds each
219 with 3 repetitions in the core and rim parts of 4-5 spinel grains within one thin
220 section. Measurement conditions were 15 kV and 60 nA using TAP crystal for
221 intensities at flank positions and with remaining 4 spectrometers were measured
222 chemical composition at the same spot simultaneously. Averaged $\text{FeL}\alpha$ and $\text{FeL}\beta$
223 intensities for one sample were used to calculate iron oxidation state of spinel from
224 the equation obtained after standardization, where $\text{FeL}\beta/\text{FeL}\alpha$ ration and FeO total
225 content correlate with $\text{Fe}^{3+}/\Sigma\text{Fe}$ measured by Mössbauer spectroscopy.

226 Owing to the lack of an appropriate geobarometer for spinel peridotites, the assumed
227 equilibrium pressure for oxygen fugacity calculations has been set at $P = 1.5$ GPa.
228 Equilibrium temperatures have been calculated using coexisting minerals and the Ca-
229 in-orthopyroxene geothermometer of Brey and Köhler (1990) and olivine-spinel
230 geothermometer of Li et al. (1995).

231

232 4. Results

233

234 4.1 HSE and chalcophile elements in spinel and plagioclase lherzolites

235

236 HSE and chalcophile element compositions of the New Caledonia lherzolites are
237 reported in Table 1 and displayed in Fig. 2, 3, 4. Spinel and plagioclase lherzolites are
238 relatively homogeneous in terms of HSE, Se, Te concentrations, abundance patterns
239 and Os isotopic compositions, with plagioclase-bearing samples showing
240 indistinguishable patterns from those of spinel lherzolites. The concentrations of the
241 highly siderophile and chalcophile elements are in the range of those observed for
242 modern abyssal and ophiolitic peridotites, displaying good correlation for Ir group PGE
243 (IPGE, e.g., Os vs. Ir and Ir vs. Ru) and more dispersed variations for the Pt group
244 PGE (PPGE, Fig. S3). In primitive mantle (PM) normalised concentration diagrams
245 (Fig. 3), the lherzolites exhibit flat or gently sloping patterns with similar PM-
246 normalized PGE concentrations and depletions in Au (except for sample BAB2B) and
247 Re compared to the PGE (with the exception BAB2B for Au and POU1A and POU3 for
248 Re). Overall, absolute contents of the PGE are similar or slightly lower than primitive
249 mantle (PM) values (Becker et al., 2006; Fischer-Gödde et al., 2011), overlapping the
250 field of the abyssal peridotites and peridotite tectonites from continental settings
251 (e.g., Fig. 2 and Becker and Dale, 2016). Ru/Ir and Pd/Ir ratios are suprachondritic,
252 as observed for other mantle lherzolites (e.g. Lorand et al., 1999; Rehkämper et al.,
253 1999; Luguet et al., 2003; Becker et al., 2006).

254 Initial $^{187}\text{Os}/^{188}\text{Os}$ ratios calculated at 53 Ma (i.e. the inferred age of initial magmatism
255 in the subduction system, e.g. Cluzel et al., 2006) vary from chondritic to slightly
256 suprachondritic (0.1273-0.1329, Fig. 4a), corresponding to $\gamma_{\text{Os}(53\text{Ma})}$ of 0.5 to 4.9.
257 These values overlap with data of abyssal peridotites and orogenic peridotites, but
258 tend to be somewhat higher than for other mantle lherzolites bearing comparable

259 depletion degrees (Fig. 4a and 4b). $^{187}\text{Re}/^{188}\text{Os}$ ranges from subchondritic to slightly
260 suprachondritic values (0.186-0.525, see Fig. 4c).

261 Se and Te are positively correlated in the lherzolites (Fig. 5a) and range between 54 -
262 91.3 ng/g and 7.3 - 13.8 ng/g, respectively. Se/Te ratios (5.9-7.1) are slightly lower
263 than the PM value and similar to the data previously obtained on depleted lherzolites
264 (Wang and Becker, 2013). Se and Te do not display any correlation with PGE
265 abundances, with the exception of Te, which shows a weak correlation with Pd (Fig.
266 5b). S contents are high and variable (202 - 1268 $\mu\text{g/g}$) compared to unserpentinised
267 peridotites, leading to high S/Se ratios (2703-16289, Fig 5c).

268

269 4.2 HSE and chalcophile elements in harzburgites

270

271 On the basis of HSE behaviour and Os isotopic compositions (Fig. 2, 3 and 6, Table 1),
272 the studied harzburgites can be grouped into two different sub-types: type-A and
273 type-B.

274 *Type-A harzburgites* (TI1, TI2, PO4 and YA1) are characterised by notably lower mass
275 fractions of all PGE and most other chalcophile elements (Figs. 2, 4) and more
276 fractionated HSE and chalcophile element patterns (Fig. 6a) compared to the
277 lherzolites. Mass fractions of the PGE in these harzburgites are 1.07-2.07 ng/g for Os,
278 0.50-1.14 ng/g for Ir, 1.53-2.52 ng/g for Ru, 0.19-0.27 ng/g for Rh, 2.42-2.70 ng/g
279 for Pt and 0.49-0.57 ng/g for Pd. Among the sub-group A, sample YA1 displays
280 distinct PGE abundances, showing much lower Os, Ir, Pt, Pd contents (0.55 ppb for
281 Os, 0.30 ppb for Ir, 0.27 ppb for Pt and 0.26 ppb for Pd), with exceptions for Ru, Rh,
282 Au and S.

283 HSE and chalcophile element diagrams of type-A harzburgites display fractionated
284 patterns, with concentrations decreasing towards Re. Os and Ru are enriched

285 compared to Ir, leading to correlated suprachondritic Os/Ir and Ru/Ir ratios
286 (Os/Ir=2.9-7.9; Ru/Ir=1.8-2.1, Fig. 4). Pt and Au generally show positive spikes,
287 more pronounced for Au, with the exception of YA1, which displays a negative Pt
288 anomaly. Pd contents are low (< 0.1 PM values) and constant for PO4, TI1, TI2, with
289 Pd/Ir showing subchondritic ratios for all studied samples. Positive correlations are
290 observed between IPGE (Fig. 2a-b-c) and Pt-Ir (not shown), and, somewhat
291 surprisingly, between IPGE and the fertility indicators (i.e. Al₂O₃ and CaO, not shown).
292 Mass fractions of Te, Se and S are low, often close to or below the detection limit,
293 again with the exception of the harzburgite YA1.

294 For all type-A harzburgites, Re concentrations are very low (about 0.02 ng/g), leading
295 to subchondritic ¹⁸⁷Re/¹⁸⁸Os ratios (0.045 to 0.196, the latter value also reflecting the
296 low Os concentrations in YA1). Os isotopic compositions are subchondritic to chondritic
297 (0.1203-0.1266, corresponding $-5 \leq \gamma_{\text{Os}(53 \text{ Ma})} \leq -0.1$) and do not define any
298 correlation with ¹⁸⁷Re/¹⁸⁸Os or incompatible element depletion indices (i.e. Al₂O₃, see
299 Fig. 4).

300

301 *Type-B harzburgites* comprise very fresh samples from Kopeto (KPT2, KPT3, KPT5),
302 Poro (PO3) and Poya (PY1) massifs. Compared to type-A harzburgites, these samples
303 have much lower HSE abundances and display variable and strong fractionations
304 among PGE and more incompatible chalcophile elements (Fig. 2 and 6b). In detail, Os,
305 Ir and Pt show positive correlations (Fig. 2) and are strongly depleted compared to
306 Ru, Rh and Pd (Os= 0.003-0.071 ppb, Ir= 0.015-0.079 ppb, with Os/Ru=0.01-0.26
307 and Ru/Ir= 2.5-20). For sample PY1, Pt is enriched relative to IPGE, Rh and Pd
308 (Pt/Rh=7.7; Pt/Pd=5.5). Pd, Re and S-Se-Te have similarly low normalized
309 abundances, with chalcophile elements often close to or below the detection limit. Au

310 exhibits positive spikes for PY1, KPT3 and PO3 samples and tends to be more enriched
311 than similar incompatible chalcophile elements (i.e. Pd and Re).

312 Measured $^{187}\text{Os}/^{188}\text{Os}$ ratios vary from chondritic to suprachondritic (0.1273-0.1534)
313 and are coupled with high and variable $^{187}\text{Re}/^{188}\text{Os}$ (1.62-32). Initial Os isotopic
314 compositions calculated at 53 Ma range from depleted to slightly suprachondritic
315 values ($0.1181-0.1365$, $-7 \leq \gamma_{\text{Os}(53\text{Ma})} \leq 3$).

316 Replicate analyses of samples PY1, KPT2, KPT5, PO3 yield quite similar results for Ru
317 ($< 5\%$ relative deviation, except for sample KPT2) and Au ($\sim 6\%$ for PY1 and KPT5)
318 and acceptable results for Pt for PY1-KPT5 (11.5 - 14.0 % relative deviation). Values
319 appear much more scattered for Os and Re ($\text{RSD} > 30\%$) and less dispersed for Rh
320 and Pd ($7 \leq \text{RSD}\% \leq 32$). The relative deviation of chalcophile elements is more limited,
321 mostly $< 15\%$.

322 The large variations of mass fractions of HSE and chalcophile elements in duplicate
323 samples reflects the very low mass fractions of these elements combined with the
324 inhomogeneity in the distribution of HSE carrier phases in gram-size quantities of rock
325 powder, an issue that has already been recognised in peridotitic rocks (e.g. Becker et
326 al., 2006; Luguet et al., 2007).

327

328 4.3 Oxybarometry

329

330 Geothermometric estimates and calculated oxygen fugacity values are reported in
331 Table 2. Equilibrium temperatures calculated for porphyroclastic assemblies with the
332 Ca-in-orthopyroxene thermometer (Brey and Köhler, 1990) range between 930-
333 1130°C, with samples YA1 and TI2 displaying the lowest temperatures (930°C-980°C,
334 see Table 2). Olivine-spinel geothermometry (Li et al., 1995) yields considerably lower
335 equilibration temperatures (815-940°C).

336 Oxygen fugacity estimated with the Wood (1990) method yielded values close to the
337 FMQ (fayalite-magnetite-quartz) buffer for all the harzburgites ($0.16 \leq \Delta \log \text{FMQ}$
338 ≤ 0.71). Similar estimates ($0.18 \leq \Delta \log \text{FMQ} \leq 0.76$) are obtained using temperatures
339 calculated with the olivine-spinel geothermometer. No significant difference can be
340 observed between sub-group A and B harzburgites. Remarkably, the highest oxygen
341 fugacity values are recorded by two harzburgites belonging to sub-group A (YA1 and
342 TI2), which are characterised by lower degrees of depletion, as inferred from trace
343 element modelling (see Secchiari et al., 2019a).
344 By contrast, lherzolite BA1 lherzolite indicates much more reducing oxygen fugacity
345 conditions ($\Delta \log \text{FMQ} \leq -3.73$).

346

347 5 Discussion

348

349 5.1 HSE and Re-Os systematics of the lherzolites

350

351 Major element composition and lithophile trace element chemistry of spinel lherzolites
352 indicate moderately depleted compositions, inherited from low partial melting degrees
353 (8-9%) of a DMM source, whereas plagioclase lherzolites originated through reactive
354 melt percolation of spinel lherzolites by highly depleted, incremental melt fractions of
355 a DMM source in the shallow lithosphere (Secchiari et al., 2016). In the following
356 sections the processes that may have affected HSE and Os isotopic signature of the
357 New Caledonia lherzolites will be discussed: low temperature alteration, in particular
358 serpentinisation, partial melting and the role of melt infiltration and chemical
359 disequilibrium of the HSE in mantle rocks.

360

361 5.1.1 Effects of serpentinisation on HSE and $^{187}\text{Os}/^{188}\text{Os}$

362

363 Serpentinisation is a widespread process of hydrothermal alteration in ultramafic
364 lithologies. However, its influence on HSE behaviour has not been investigated with
365 much detail, despite some authors have proposed it as a possible cause for ^{187}Os
366 ingrowth and Re variations in the upper mantle (Snow and Reisberg, 1995; Walker et
367 al., 1996; Standish et al., 2002). Recent experimental studies have shown that during
368 serpentinisation the formation of secondary sulphides, Fe-Ni alloys and native metals
369 (Au-Cu) is promoted by reducing f_{O_2} conditions (Klein and Bach, 2009; Foustoukos et
370 al., 2015) and thus, with the exception of Au, HSE may be retained in the host rock.
371 Comparison of partially serpentinised and unserpentinised peridotites displaying
372 similar major element features supports the notion that at least PGE ratios are little
373 changed by moderate to strong serpentinisation (Becker and Dale, 2016).

374 The New Caledonia Iherzolites underwent intermediate serpentinisation (LOI = 6.4 to
375 10.7 %, see paragraph 2.1 and Table 1), which had limited effects on the budget of
376 fluid immobile moderately incompatible lithophile trace elements in these rocks
377 (Secchiari et al., 2016). Notably, PGE contents and ratios in the Iherzolites are similar
378 to other unaltered and serpentinised Iherzolites from the modern oceans and ophiolitic
379 complexes (see Fig. 2 and 3 e.g.; Snow et al., 2000; Luguet et al., 2001, 2004 ;
380 Pearson et al., 2004; Alard et al., 2005; Becker et al., 2006; Fischer-Gödde et al.,
381 2011; Becker and Dale, 2016). This observation supports the hypothesis that PGE
382 abundances are comparable in fresh and variably serpentinised ultramafic rocks
383 (Becker et al., 2006; Liu et al., 2009; Fischer-Gödde et al., 2011; Marchesi et al.,
384 2013; Becker and Dale, 2016), implying that serpentinisation results in minor changes
385 in PGE ratios.

386 By contrast, the possible influence of serpentinisation on Au and Re is more difficult to
387 evaluate, as no study has systematically investigated its effect on the behaviour of the
388 aforementioned elements. In the lherzolites from New Caledonia, Au displays similar
389 normalized concentrations as Re and, with the exception of a few samples, both
390 elements are depleted relative to Pd, Te and Se. Au abundances tend to be somewhat
391 lower than abundances in other lherzolites with similar major element composition
392 (Fig. 3). Although the compositions can be entirely explained by magmatic
393 fractionation processes (see subsequent chapters), minor losses of Au due to
394 hydrothermal alteration cannot be ruled out (e.g. Lorand et al., 1999). The lack of
395 correlation between Au and Al₂O₃ (not shown) could be a hint that Au abundances
396 may have been affected by a combination of magmatic processes and serpentinisation
397 (i.e. Fischer-Gödde et al., 2011). Rhenium is slightly depleted compared to the PGE
398 for most of the studied lherzolites, but displays higher concentrations than other
399 mantle lherzolites (Fig. 3). In addition, Re contents do not correlate with LOI and
400 Re/Os ratios cover the range generally reported for moderately depleted mantle rocks.
401 The samples with the lowest Re contents display the highest LOI values, suggesting
402 that no significant quantities of Re were added during the interaction with seawater
403 during serpentinisation. Likewise, the chondritic to slightly suprachondritic ¹⁸⁷Os/¹⁸⁸Os
404 cannot be ascribed to serpentinisation, as unrealistically high water-rock ratios (~
405 10³-10⁴) would be required in order to perturb the whole rock ¹⁸⁷Os/¹⁸⁸Os at the %
406 level or higher (e.g. Becker and Dale, 2016). The lherzolite data also shows mass
407 fractions of Se and Te and Se/Te that are similar to values in unserpentinised
408 lherzolites (e.g., Wang and Becker, 2013). In contrast sulfur in most lherzolites from
409 New Caledonia shows much higher concentrations than typical for peridotites, which is
410 readily explained by contamination with seawater-derived sulfur during
411 serpentinisation.

412 We thus conclude that the HSE (perhaps with the exception of Au), Se, Te and Re-Os
413 signature of the lherzolites offer no conclusive evidence that serpentinisation and
414 associated reactions affected these elements in a noticeable way.

415

416 5.1.2 Partial melting and chemical disequilibrium of the HSE in the mantle

417

418 Spinel and plagioclase lherzolites exhibit comparable HSE contents and patterns,
419 similar to other lherzolites from oceanic or continental settings that underwent low to
420 moderate degrees of melt extraction (Fig. 2 and 3).

421 Partial melting has often been invoked as a possible cause for HSE and $^{187}\text{Os}/^{188}\text{Os}$
422 variations in mantle rocks (e.g. Reisberg and Lorand, 1995; Meisel et al., 2001).

423 Studies of the behaviour of the HSE during mantle melting and their abundances in
424 mantle rocks have supported the hypothesis that HSE concentrations in residual
425 peridotites result from sulphide-silicate partitioning during magmatic processes (i.e
426 Becker and Dale, 2016; Brenan et al., 2016 and references therein) and that at
427 temperatures relevant for mantle processes homogeneous sulphide liquid and, in
428 special cases, sulfide solid solutions, coexist in equilibrium with silicate melt, olivine,
429 pyroxenes and an Al-rich phase (e.g. Rehkämper et al., 1999; Mungall and Brenan,
430 2014; Brenan et al., 2016). Experimentally determined sulphide melt-silicate melt
431 partition coefficients ($D^{\text{sulph/sil}}$) for PGE have been shown to be high and constant (10^5
432 to 10^6 , e.g. Mungall and Brenan 2014; Brenan et al. 2016), while Au shows slightly
433 lower $D^{\text{sulph/sil}}$ ($\sim 10^4$). Therefore, up to moderately high degrees of melting, PGE
434 behave as compatible elements and their inter-elemental ratios remain similar as long
435 as sulphide is present in the mantle residue. By contrast, Re is much less chalcophile
436 ($D^{\text{sulph/sil}} \sim 300-800$, e.g. Fonseca et al., 2007; Brenan, 2008) and is expected to
437 become more quickly depleted in the residual mantle.

438 Major element compositions of sulphides in the spinel lherzolites (Table S1) are
439 consistent with a residual origin after incongruent melting processes (e.g. Bockrath et
440 al., 2004; Ballhaus et al., 2006). The occurrence of homogeneous monosulphides also
441 suggests relatively high cooling rate after the melting event.

442 Overall, the studied lherzolites are characterised by flat to gently sloping PGE
443 patterns, with similar PM-normalized abundances, no PPGE fractionation and nearly
444 constant ratios for IPGE (i.e. Os/Ir, Ru/Ir). By contrast, Au and Re display the
445 strongest depletion. These features imply that HSE, with the exception of Au and Re,
446 exhibit a similar compatible behaviour during mantle melting, as expected for low to
447 moderate melting degrees in presence of residual sulphide melt. This observation is
448 consistent with the previous estimates obtained through geochemical modelling
449 (Secchiari et al., 2016) and with the occurrence of a residual subsolidus sulphide
450 assemblage in spinel lherzolites.

451 Although the PGE patterns are nearly flat, with only slight depletion of Pd in a few
452 samples, the depletion of Au and Re, the range of chondritic to slightly suprachondritic
453 $\gamma^{187}\text{Os}_i$ and the higher mass fractions of Se and Te compared to Re and the other HSE
454 suggest a multi-stage history of the lherzolites. Notably, $\gamma^{187}\text{Os}_i$ do not correlate with
455 mass fractions of incompatible HSE such as Re, Re/Os nor with fertility indicators (Fig.
456 4), as was observed in some other suites of lherzolites (Becker and Dale, 2016).

457 The Os isotopic signature may be a pre-existing feature of the mantle source, i.e.
458 already present before the recent melt extraction event (Secchiari et al., 2016). This
459 is supported by the dispersed Os isotopes-fertility indicators trends, as well as by
460 some old model ages recorded by our lherzolite samples ($T_{\text{MA}}(\text{PM}) = 0.4\text{-}0.8$ Ga, see
461 Table 1). In addition, the remarkable absence of magmatic Cu-Fe-rich sulphides (e.g.
462 see Lorand et al., 2013) argue against a recent, post-melting sulphide addition. We
463 thus speculate that the bulk HSE, Se, Te and Os isotope compositions of the

464 lherzolites are the result of partial melting event which affected a mantle source
465 previously characterised by an heterogeneous sulphide population including both
466 residual and magmatic sulfides precipitated along grain boundaries by infiltrating
467 melts (Burton et al., 1999; Lorand et al., 1999; Alard et al., 2000, 2002).

468

469 5.2 Sulphur, Se and Te behaviour in the New Caledonia lherzolites

470 Sulfur mass fractions are variable in the lherzolites from New Caledonia and typically
471 much higher compared to estimates of the depleted MORB mantle source (DMM ~
472 150-200 ppm, Mathez, 1976; Salters and Stracke, 2004) and mass fractions of S in
473 unaltered lherzolites (e.g., Wang and Becker, 2013). In addition, sulphur does not
474 correlate with fertility indicators (i.e. Al_2O_3), as commonly observed in unserpentinised
475 mantle tectonites (e.g., Lorand and Alard, 2010; Wang and Becker, 2013). The high S
476 concentrations and the lack of correlation with melting indicators suggest that S was
477 added late in the evolution of the rocks. The sulphur budget of mantle peridotites can
478 be strongly influenced by seawater-rock interaction, because of the high sulphate
479 content of seawater, leading to hydrothermal sulphides and sulphate precipitation (Alt
480 and Shanks, 1998). We note that the major element chemistry indicates a residual
481 origin for the sulphide phases of the lherzolites (see paragraph 4.1 and 5.1.2).
482 Hydrothermal sulphides or sulphates could not be identified.

483 Recent geochemical works have demonstrated the role of serpentine as a sink of S
484 under various oxidation states (S^{2-} , S^- , S^0 and S^{6+} , Debret et al., 2017). These
485 studies have shown that S concentrations can be anomalously high in serpentinised
486 peridotites (up to 1 wt.%, see Alt et al., 2003), as S can be accommodated in
487 serpentine minerals, accounting from 60 to 100% of the sulphur budget of the
488 peridotite (Debret et al., 2017). In situ analysis of serpentine minerals have revealed
489 that S can be hosted in nano-phases associated with serpentine or trapped either via

490 Si substitutions in the tetrahedra, or as a sulphate ion in the network of the
491 tetrahedral sheet of serpentine minerals (Debret et al., 2017).

492 The addition of S during serpentinization is also reflected in the high suprachondritic
493 S/Se ratios (up to 16500) and the excellent correlation observed between S
494 concentrations and S/Se ratios (see Fig. 5c). Despite the strong S enrichments, Se
495 and Te display 'normal' concentrations and Se/Te ratios are in the range of other
496 Iherzolites (see Wang and Becker, 2013). These data confirm that Se-Te contents and
497 ratios were not significantly impacted by serpentinisation, as previously observed for
498 other peridotites that experienced low to moderate serpentinisation degrees (e.g.
499 Wang and Becker, 2013; Marchesi et al., 2013).

500 Moreover, Se-Te show a good correlation between each other (Fig. 5a), implying that
501 they are controlled by the same mineral phases. In mantle peridotites, Se can replace
502 S as a chalcogen anion within the crystalline structure of sulphides (e.g. Bulanova et
503 al., 1996; Hattori et al., 2002; Helmy et al., 2010) or can form Se-rich micro phases,
504 while Tellurium, owing to its semi metal nature, tends to partition between sulphides
505 and late exsolved micrometric tellurides (Pt, Pd, Te, As, Bi phases). The latter are
506 thought to crystallise at low temperatures during cooling, once sulphide melt becomes
507 saturated with respect to Te (Luguet et al., 2004; Lorand et al., 2008; Lorand and
508 Alard, 2010). In the Iherzolites, Se and Te do not correlate with melting indicators,
509 but Te displays a rough positive correlation with Pd (Fig. 5b), which suggests that the
510 sulphide melt-bulk silicate partition coefficient of Te should be between Se and Pd
511 (e.g., Figs. 3, 4, 5).

512

513 5.3 Type-A harzburgites: highly siderophile element systematics of a residual sub-arc
514 mantle section

515

516 The distinct HSE patterns and Os isotopic signature recorded by the New Caledonia
517 harzburgites hint that they experienced a different history compared to the northern
518 Iherzolites.

519 Three of the four samples belonging to the sub-group A (TI1, TI2, PO4) show similar
520 HSE patterns and chalcophile elements depletion, indicating that the same processes
521 contributed to the HSE and chalcophile element budget of these rocks. The low
522 chalcophile element concentrations, close to or below the detection limit, coupled with
523 low Pd/Ir ratios and subchondritic $^{187}\text{Os}/^{188}\text{Os}_i$, point out that type-A harzburgites are
524 residues of high degree of melt extraction, where sulphides melts must have been
525 nearly completely dissolved in coexisting silicate melt.

526 Experimental studies have in fact predicted a compatible behaviour for all the PGE
527 during mantle melting as long as sulphide is retained in the peridotite (Mungall and
528 Brenan, 2014). Depending on the initial S content of the mantle rocks, ~12-20% of
529 melting is required for sulphide exhaustion (Lorand et al., 1999; Luguet et al., 2007;
530 Brenan et al., 2016). As melting proceeds, sulphides are progressively dissolved into
531 the melt and the PGE become concentrated in the residual sulphide melt (Mungall and
532 Brenan, 2014). Provided that chemical equilibrium is attained, increasing degrees of
533 partial melting should slightly increase whole rock PGE contents, but element ratios
534 should remain almost constant. At the point when sulphide is completely removed,
535 IPGE and Pt are accommodated in metallic alloys, while Re, Au and Pd mass fraction
536 should become extremely low, as these elements are not hosted in any residual
537 mantle phase (Mungall and Brenan, 2014). Hence for high melting degrees, the
538 abundances of the HSE in the residue should reflect mineral-melt partitioning and the
539 P-T and f_{O_2} -dependent solubility of Pt and IPGE alloys in silicate melt (Fonseca et al.,
540 2011, 2012; Mungall and Brenan, 2014; Brenan et al., 2016).

541 The IPGE-PPGE fractionation and the resolvable fractionations between specific PGE
542 displayed by the type A harzburgites bear witness of the high melting degrees, which

543 resulted in the formation of a S-free mantle residue. The fractionated Os-Ir-Ru-Rh
544 segments of HSE patterns and the positive Pt anomalies in type A harzburgites are
545 likely carried by residual sulphides (i.e. laurite) and metallic alloys (Os-Ir and Pt-Ir,
546 see Lorand et al., 1999; Luguet et al., 2001, 2007). These latter are thought to
547 precipitate from sulphide melt shortly before the complete exhaustion of sulphide
548 (Mungall and Brenan, 2014) or immediately after sulphide consumption, due to f_{S_2}
549 lowering and diminished metal-sulphide complexation in the silicate melt (Fonseca et
550 al., 2012). The variable, but broadly systematic inter-element fractionation among the
551 IPGE (high Os/Ir and Ru/Ir), high Ru/Rh and the variable Pt anomaly relative to Rh
552 and Pd indicate the different proportions of residual Ir-Pt alloys in different samples
553 and preferred retention of Ru and Os relative to Ir in the residual PGE alloys (e.g.
554 Brenan and Andrews, 2001; Fonseca et al., 2012).

555 The HSE fractionations of type A harzburgites are different from HSE patterns of
556 modern harzburgites from MOR environments (Fig. 6a), as the latter are characterised
557 by flat or weakly fractionated Os-Ir-Ru triplet and they rarely display positive Pt spikes
558 (Snow and Schmidt, 1998; Luguet et al., 2001, 2003). By contrast, HSE elemental
559 fractionations of type-A harzburgites are similar to patterns of some arc xenoliths
560 (Saha et al., 2005; Liu et al., 2015; Scott et al., 2019) or ophiolitic peridotites bearing
561 a supra-subduction zone signature (see Büchl et al., 2002, 2004; O'Driscoll et al.,
562 2012). Similar fractionations have been reported for some mantle xenoliths from the
563 Chatam Islands (New Zealand) and from some other areas (Pearson et al., 2004).

564 On the other hand, geochemical modelling based on lithophile incompatible elements
565 has shown that the extreme depletion in trace element contents displayed by the New
566 Caledonia harzburgites was achieved through a polyphase evolution, including a first
567 melting event in a mid-ocean ridge setting, followed by fluid-assisted melting
568 reaching clinopyroxene exhaustion after involvement in a subduction system (see
569 Secchiari et al., 2019a). Such high melting degrees are permissible in supra-

570 subduction zone environments, where hydrous conditions at relatively low pressures
571 can produce melt fractions substantially exceeding 20% without invoking extremely
572 high temperature (e.g. see Ulmer, 2001). Likewise, the observed LREE and FME (Sr,
573 Ba, Pb) enrichments coupled with variable Pb isotope compositions of the Type A
574 harzburgites may be explained by syn- and post-melting interactions with different
575 subduction-related components, possibly aqueous fluids and melts originated in the
576 forearc setting (Secchiari et al., 2019 a,b).

577 We thus conclude that the HSE and chalcophile element signature displayed by TI1,
578 TI2 and PO4 predominantly reflect high degrees of melt extraction, presumably in a
579 supra-subduction zone environment. The positive Pt spikes suggest that Pt-rich alloys
580 were stable in the mantle residue and were only in part dissolved in the melt during
581 melt extraction.

582 The enrichments of Au are modest (0.2-1.3 ng/g Au) and must be related to fluid
583 overprint, either from slab-derived fluids (McInnes et al., 1999; Kepezhinskis et al.,
584 2002) or from low-T alteration, e.g., during obduction (e.g. Snow et al., 2000).

585 The harzburgite YA1 shows higher S and Se concentrations (Fig. 5a), which,
586 considering the significant LOI value of 6.83%, could be related to serpentinisation
587 and precipitation of secondary sulphides. The strongly fractionated HSE pattern and
588 the low concentrations of the incompatible HSE (i.e. Pd, Re) indicate that the HSE
589 budget of YA1 is also governed by melting, as for TI1, TI2 and PO4 harzburgites. The
590 low Os, Ir and Pt concentrations, are much closer to the values reported for type-B
591 harzburgites (see Table 1 and Fig. 5b). Sample YA1 can thus be seen as transitional
592 between type-A and type-B sub-group.

593

594

595 5.4 Origin of type-B harzburgites – strong depletion followed by subduction zone
596 metasomatism?

597

598 Type-B harzburgites mostly occur in the central massifs, however one sample (PO3)
599 has also been identified in the eastern zone, close to the area where one type-A
600 harzburgite (PO4) was sampled. Type-B harzburgites display remarkably different HSE
601 and Re/Os behaviour compared to type-A sub-group (Fig. 2 and 6), indicating that
602 different processes need to be invoked in their genesis.

603 Type-B harzburgites show low abundances of incompatible chalcophile elements, i.e.
604 Pd, S, Se and Re, with values in the range of type-A harzburgites. In principle such
605 low concentrations could be reconciled with high melting degrees and sulphide
606 exhaustion in the mantle source. The strong depletion of Os, Ir and Pt, (Fig. 6b)
607 coupled with slightly subchondritic to suprachondritic $^{187}\text{Re}/^{188}\text{Os}$ (0.23 to 37) and
608 $^{187}\text{Os}/^{188}\text{Os}$ (0.1239 to 0.302) are remarkable and do not occur in residual
609 harzburgites from convecting mantle, as represented by abyssal peridotites.

610 The HSE in type-B harzburgites share similarities with some xenoliths from arc
611 settings such as low Os contents associated with chondritic to suprachondritic
612 $^{187}\text{Os}/^{188}\text{Os}$ (Brandon et al., 1996, 1999; Saha et al., 2005; Widom, 2011). These
613 features have been ascribed to interactions with subduction zone fluids (i.e. fluids
614 from subducted altered oceanic crust and/or its sedimentary cover), which may have
615 induced sulphide breakdown in the residual arc mantle, locally modifying the Os
616 isotopic signature of the mantle (Wisdom et al., 2003). Such qualitative observations
617 have also been supported by experimental works, that highlighted the critical
618 influence of oxygen fugacity (f_{O_2}) on sulphide and alloy stability (e.g. Andrews and
619 Brenan, 2002; Fonseca et al., 2011, 2012; Mungall and Brenan, 2014).

620 Moreover, the strongly fractionated, IPGE-depleted, HSE patterns displayed by type-B
621 harzburgites closely resemble those observed in some refractory harzburgites and
622 replacive dunites that underwent interaction with S-undersaturated melts in some
623 ophiolites (Büchl et al., 2002; Lorand et al., 2004).

624 As metasomatism by subduction fluids and hydrous melts has been proposed for the
625 New Caledonia harzburgites based on isotopic and incompatible element studies, we
626 have determined oxygen fugacities on a set of five harzburgites and one lherzolite, in
627 order to test if the different HSE signature of type-B harzburgites could reflect higher
628 f_{O_2} conditions. As a whole, the harzburgites record more oxidised conditions compared
629 to the lherzolite (see Table 2). This is consistent with the hypothesis that the
630 lherzolites represent slightly depleted mantle rocks not directly involved in the Eocene
631 subduction system (Secchiari et al., 2016). However, the harzburgites exhibit f_{O_2}
632 values close to the FMQ buffer and in the range of the suboceanic mantle (e.g.
633 Bryndzia and Wood, 1990). Also, type A harzburgites tend to be slightly more oxidised
634 than type B harzburgites.

635 The relatively low oxygen fugacity values may be related to the high depletion
636 experienced by the harzburgites. A recent study of B nard and coauthors (2018) has
637 in fact shown that increasing melt depletion at un-buffered f_{O_2} conditions can induce
638 oxygen fugacity variation in the sub-arc peridotites, as Fe^{3+} is more extensively
639 extracted than Fe^{2+} as melting proceeds, producing residues with lower $Fe^{3+}/\Sigma Fe$ than
640 in the original mantle source. We note that the most depleted harzburgites (i.e. type-
641 B PY1, KPT5 and PO3) in our dataset yield the lowest computed oxygen fugacities.
642 Following this interpretation, we suggest that the harzburgites recorded higher f_{O_2}
643 conditions compared to the lherzolites due to fluid-assisted melting and interaction
644 with an oxidising component, but increasing degrees of melt extraction from type A to
645 type B harzburgites possibly led to progressive lowering of f_{O_2} .

646 Alternatively, calculated oxygen fugacity values may partly reflect f_{O_2} conditions
647 related to the melting conditions of the harzburgites in the suboceanic mantle (Lee et
648 al., 2005). From this perspective, one may speculate that the oxidising capacity of
649 slab-derived fluids or melts was not high enough to erase the memory of the original
650 f_{O_2} conditions. For the New Caledonia archipelago, Eocene subduction started close to

651 or in correspondence of an active oceanic spreading center, where hot and young (~
652 6-9 My old, Cluzel et al., 2016) lithosphere was forced to subduct. In such a context,
653 fluid fluxes from the downgoing slab must have been limited, due to the young age of
654 the subducted material and the intra-oceanic nature of the subduction (Cluzel et al.,
655 2016). In addition, post-melting metasomatism is thought to have occurred through
656 interaction with small fractions (0.5-1%) of boninitic magmas, which may have not
657 been able to maintain their oxidising capacity during percolation through the sub-arc
658 mantle.

659 In conclusion, the effect of f_{O_2} on the different HSE patterns of type A and B
660 harzburgites is unclear, and perhaps insignificant, as their difference in $\Delta \log f_{O_2}$ is
661 minor. Thus, most likely the stronger fractionation and depletion of some IPGE in type
662 B harzburgites reflects the higher degrees of melting.

663

664 5.5 Type-B harzburgites: a broader perspective

665

666 Despite being similar in terms of chemistry or mineralogy, type-A and B harzburgites
667 possess distinct HSE signatures. In addition, the HSE signatures of type-B harzburgites
668 have not yet been identified in other mantle tectonites, either from modern oceanic
669 lithosphere or ophiolitic complex.

670 However, similar compositions have been recently reported for some moderately
671 depleted to highly refractory peridotites and mantle xenoliths from New Zealand
672 (Scott et al., 2019). The New Zealand mantle is composed of isotopically
673 heterogeneous mantle fragments with evolutionary histories extending over 2.75 Ga
674 (Os model ages= 0.1-2.75 Ga, with a broad peak at 1.2 Ga), and PGE systematics
675 decoupled from major element compositions (see Scott et al., 2019; Liu et al., 2015).
676 These features have been explained by accretion of Zealandia lithospheric mantle

677 from amalgamation of genetically unrelated convecting mantle fragments which were
678 swept together beneath the Gondwana subduction margin, variably re-melted and
679 laterally accreted (Scott et al., 2019).

680 Among the New Zealand peridotite suites, mantle xenoliths from Lake Moana and
681 Chatam Island show HSE patterns that are similar to our dataset (Fig. 8). Lake Moana
682 Cretaceous xenoliths include cpx-free harzburgites that experienced up to 30%
683 melting, while Eocene-aged Chatam Island harzburgites exhibit a less refractory
684 nature, as attested by the presence of primary clinopyroxene (up to 1.8% modal,
685 Scott et al., 2016). Such depletion degrees were achieved either by plume melting or
686 hydrous melting in an arc setting for the Lake Moana xenoliths, whereas Chatam
687 Island samples are thought to represent fragments of fore-arc lithosphere (Scott et al.,
688 2016, 2019).

689 Overall, HSE diagrams highlight that New Zealand mantle xenoliths reproduce with
690 good approximation both patterns observed in our harzburgites, namely type-A and
691 type-B (Fig. 7). IPGE patterns are broadly sub-parallel, with the New Caledonia
692 harzburgites falling within or at the lower range of values displayed by the New
693 Zealand samples, whereas Pt, Pd and Re exhibit much more variability.

694 For most of the New Zealand xenoliths, Ru concentrations are higher compared to the
695 contents in the New Caledonia harzburgites. Higher Ru contents cannot be ascribed to
696 different degrees of melting, as fertility indicators (i.e. Mg#(Ol), Cr#(Spl)) indicate
697 similar degrees of melt extraction for both peridotite suites (see Scott et al., 2016,
698 2019; Secchiari et al., 2019a). The increased Ru retention in the New Zealand
699 samples may be reconciled to the higher Cr-spinel content of these lithologies (up to
700 2.8%, see Scott et al., 2016, vs. up to 0.8% for our harzburgites). Numerous studies
701 have in fact demonstrated that spinel can be a significant host for Ru ($D^{\text{spinel/melt}} \sim 20$,
702 Capobianco and Drake, 1990). In addition, increase in oxygen fugacity markedly
703 enhances Ru compatibility in Cr-rich spinel ($D^{\text{spinel/melt}}$ up to 500 for f_{O_2} of -0.5 FMQ,

704 Park et al., 2012), which can accommodate Ru within its crystal lattice (Pagé and
705 Barnes, 2016) or as laurite and/or Ru-rich alloy inclusions (Brenan and Andrews,
706 2001). Recent geochemical works have also illustrated the importance of Ru retention
707 in the sub-arc mantle for the HSE signature of arc lavas (Dale et al., 2012; Park et al.,
708 2013). These studies explain the low Ru concentrations and the high Pt/Ru ratios of
709 the volcanic products as related to Ru retention in the mantle source due to the
710 presence of Cr-rich spinel or PGM (see Dale et al., 2012; Park et al., 2013). Likewise,
711 positive Ru anomalies in our type-B harzburgites may reflect the presence of small
712 laurite or Ru-rich phase inclusions, which could have escaped the high melting
713 degrees due to the shield effect of spinel.

714 Other HSE (e.g. Pd and Re) in the New Caledonia harzburgites display a wider range
715 of values compared to the New Zealand samples, possibly related to variable
716 proportions of traces of sulfide precipitated from silicate melt.

717 Enrichments of Pd have also been recognised in other sub-arc mantle sections, where
718 they have been attributed to slab-derived fluids metasomatism, due to the high
719 solubility of Pd in aqueous fluids (McInnes et al., 1999; Park et al., 2013). Likewise,
720 Re addition in mantle wedge peridotites may be due to Re release in slab derived
721 fluids during dehydration of the mafic portion of the subducting slab (see Dale et al.,
722 2009). Hence, we conclude that Pd-Re (as well as Te-Se-S) re-enrichments in type-B
723 harzburgites may have been facilitated by minor sulfide precipitation from slab
724 derived fluids or melts.

725 By contrast, the widespread negative Pt anomalies may reflect destabilisation of a
726 pre-existing Pt-alloy phase, possibly related to continued melting after alloy saturation
727 (see Mungall and Brenan, 2016), and Pt release into the melt.

728

729 5.6 Inferences from Re-Os systematics of the New Caledonia harzburgites

730

731 All type-A harzburgites, including YA1, show unradiogenic $^{187}\text{Os}/^{188}\text{Os}_i$ and very low
732 Re/Os relative to the range of chondritic values (Walker et al., 2002) or primitive
733 mantle estimates (Meisel et al., 1996). The γ_{Os_i} overlap with data from depleted
734 abyssal peridotites and mantle sections from some ophiolites (e.g., Becker and Dale,
735 2016).

736 In order to obtain an estimate of the time of melt depletion, we calculated Re-Os
737 model ages (T_{MA}) and Re-depletion model ages (T_{RD}). The Re-depletion model ages
738 are generally used for samples with low Re contents and Re/Os ratios. However it is
739 important to note that this method provides minimum depletion ages, as melting is
740 not expected to remove all of the Re on a whole-rock scale.

741 The Re-depletion ages for type-A harzburgites are quite homogeneous for three out
742 four samples (TI1, TI2, YA1) ranging between 0.4 and 0.7 Ga for (see Table 1), while
743 sample PO4 yields an older Re-depletion age of 1.3 Ga. The younger model ages can
744 be linked to the previous evolution of the New Caledonia mantle in relationship to the
745 eastern Australian margin, from which the New Caledonia archipelago was separated
746 *via* marginal rifting about 90 Ma ago (Cluzel et al., 2001, 2012; Whattam, 2009). The
747 ancient Re depletion age of the harzburgite PO4, on the other hand, reflects a mantle
748 domain that experienced long-term low Re/Os ratio. This age is also mirrored by Nd
749 isotopic signature, which shows a highly radiogenic value ($\epsilon_{\text{Nd}_i} = +13.32$, Secchiari et
750 al., 2019a), indicative of a mantle reservoir that underwent long-term depletion of Nd.
751 In addition, similar depletion ages (i.e. 1.2 Ga) occur in the New Zealand mantle rocks
752 (see Scott et al., 2019).

753 These results are consistent with recent Re-Os studies on abyssal peridotites and
754 mantle tectonites from ophiolitic sequences showing that the convecting mantle
755 contains harzburgite domains that underwent depletion events much older than the
756 age of peridotite processing under the ridge (e.g., Harvey et al., 2006).

757 In summary, the New Caledonia harzburgites show Re-Os systematics typical of
758 depleted upper mantle showing Early Paleozoic Os isotopic equilibration and evidence
759 for ancient depletion events (> 1.0 Ga). This multi-stage history led to the depleted
760 nature of the harzburgites and possibly resulted in their complex HSE geochemical
761 signatures.

762

763 Summary and conclusions

764

765 A Re-Os isotopes, highly siderophile and chalcophile element investigation of the New
766 Caledonia peridotites was carried out to unravel the behaviour of the aforementioned
767 elements in lherzolites and harzburgites from the New Caledonia ophiolite.

768 The lherzolites exhibit subchondritic to slightly suprachondritic $^{187}\text{Os}/^{188}\text{Os}_i$ (0.1273-
769 0.1329). PM-normalised HSE abundance diagrams are characterised by gently sloping
770 patterns showing increasing depletion towards Re-Au, similar to lherzolites that
771 experienced low to moderate melt extraction. However, the lack of correlation
772 between HSE and fertility indicators, as well as the slightly suprachondritic Os isotopic
773 ratios, argue against a simple partial melting history. Rather, the aforementioned
774 features and the presence of included and interstitial residual monosulphides possibly
775 indicate that melting occurred on a mantle domain that has previously experienced a
776 melt percolation event. The high S concentrations of the lherzolites (202-1268 ppm)
777 most likely result from late-stage seawater-rock reactions.

778 By contrast, the New Caledonia harzburgites record higher degrees of melt extraction,
779 as attested by the strikingly low, often below the detection limit, concentrations of
780 incompatible chalcophile elements. Despite their homogeneity in terms of
781 mineralogical and major element compositions, HSE patterns and Os isotopic
782 compositions indicate the occurrence of two distinct harzburgite sub-groups.

783 Type-A harzburgites are characterised by steeply plunging HSE patterns, showing
784 IPGE-PPGE and Os-Ir-Ru fractionation, coupled with low Re/Os ratios and
785 subchondritic $^{187}\text{Os}/^{188}\text{Os}_i$. The strongly fractionated HSE patterns and the positive Pt
786 anomalies, coupled with the high modelled melting degrees, indicate that melting
787 occurred under hydrous conditions in sub-arc mantle.

788 Type-B harzburgites display notably different HSE patterns, showing depleted Os-Ir
789 compared to Ru, positive anomalies and Pd-Re re-enrichments (relative to IPGE),
790 coupled with chondritic to strongly suprachondritic measured Os isotopic ratios
791 ($^{187}\text{Os}/^{188}\text{Os} = 0.127\text{-}0.153$). These features have not been yet identified in mantle
792 tectonites and might indicate Os-Ir-Pt release into silicate melt for higher partial
793 melting degrees.

794 The HSE signature carried by the studied peridotites, as well as the puzzling similarity
795 observed between the New Caledonia harzburgites and the New Zealand mantle
796 xenoliths, might attest the presence of a mantle source bearing a long lasting
797 evolution (> 1 Ga), possibly linked to the Zealandia formation.

798

799 Acknowledgements

800

801 We thank M. Feth for help and support in the clean laboratory and D. Cluzel for
802 assistance during samples collection in New Caledonia.

803 A.G. thanks Russian Science Foundation project 17-77-10103 for supporting iron
804 oxidation state investigations at Freie Universität of Berlin.

805 This work represents a continuation of the PhD project of A.S. on the New Caledonia
806 ophiolite, that has been supported by DFG funding (SFB-TRR 170 Subproject B2) and
807 Italian-PRIN prot. 2015C5LN35.

808

809 References

810

811 Ackerman, L., Walker, R.J., Puchtel, I.S., Pitcher, L., Jelínek, E., Strnad, L., 2009.
812 Effects of melt percolation on highly siderophile elements and Os isotopes in
813 subcontinental lithospheric mantle: A study of the upper mantle profile beneath
814 Central Europe. *Geochimica et Cosmochimica Acta* 73, 2400–2414.

815 Aitchison, J.C., Clarke, L., Meffre, S., Cluzel, D., 1995. Eocene arc-continent collision
816 in New Caledonia and implications for regional Southwest Pacific tectonic evolution.
817 *Geology* 23, 161–164.

818 Alard, O., Luguet, A., Pearson, N.J., Griffin, W.L., Lorand, J.P., Gannoun, A., Burton,
819 K.W., O'Reilly S.Y., 2005. In situ Os isotopes in abyssal peridotites bridge the isotopic
820 gap between MORBs and their source mantle. *Nature* 436, 1005-1008.

821 Alt, J.C., Shanks, W.C., 1998. Sulfur in serpentinized oceanic peridotites:
822 Serpentinization processes and microbial sulfate reduction. *Journal of Geophysical*
823 *Research* 103, 9917–9929.

824 Alt, J.C., Shanks, W.C., 2003. Serpentinization of abyssal peridotites from the MARK
825 area, Mid-Atlantic Ridge: Sulfur geochemistry and reaction modeling. *Geochimica et*
826 *Cosmochimica Acta* 67, 641 – 653.

827 Andrews, D.R.A., Brenan, J.M., 2002. Phase-equilibrium constraints on the magmatic
828 origin of laurite + Ru–Os–Ir alloy. *Canadian Mineralogist* 40, 1705-1716.

829 Becker, H., Dale, C., 2016. Re–Pt–Os Isotopic and Highly Siderophile Element
830 Behavior in Oceanic and Continental Mantle Tectonites. *Reviews in Mineralogy and*
831 *Geochemistry*, 369-440

832 Becker, H., Horan, M.F., Walker, R.J., Gao, S., Lorand, J.P., Rudnick, R.L., 2006.
833 Highly siderophile element composition of the Earth 's primitive upper mantle :
834 Constraints from new data on peridotite massifs and xenoliths. *Geochimica et*
835 *Cosmochimica Acta* 70, 4528–4550.

836 Bénard, A., Woodland, A.B., Arculus, R.J., Nebel, O., McAlpine, S.R.B., 2018. Variation
837 in sub-arc mantle oxygen fugacity during partial melting recorded in refractory
838 peridotite xenoliths from the West Bismarck Arc. *Chemical Geology* 486, 16–30.

839 Birck, J.L., Barman, M.R., Capmas, F., 1997. Re-Os Isotopic Measurements at the
840 Femtomole Level in Natural Samples. *Geostandards and Geoanalytical Research* 21,
841 19–27.

842 Brandon, A.D., Creaser, R.A., Shirey, S.B., Carlson, R.W., 1996. Osmium recycling in
843 subduction zones. *Science* 272, 861– 864.

844 Brandon, A.D., Norman, M.D., Walker, R.J., Morgan, J.W., 1999. 186Os–187Os
845 systematics of Hawaiian picrites. *Earth and Planetary Science Letters* 174, 25– 42.

846 Brandon, A.D., Snow J.E., Walker R.J., Morgan J.W., Mock, T.D., 2000. 190Pt-186Os
847 and 187Re-187Os systematics of abyssal peridotites. *Earth and Planetary Science*
848 *Letters* 177, 319-335.

849 Brenan, J.M., Andrews, D., 2001. High-temperature stability of laurite and Ru Os Ir
850 alloy and their role in PGE fractionation in mafic magmas. *Canadian Mineralogist* 39,
851 341–360.

852 Brenan, J.M., Bennett, N.R., Zajacz, Z., 2016. Experimental results on fractionation of
853 the highly siderophile elements (HSE) at variable pressures and temperatures during
854 planetary and magmatic differentiation. *Reviews in Mineralogy and Geochemistry* 81,
855 1–87.

856 Brey, G. P. & Köhler, T., 1990. Geothermobarometry in four-phase lherzolites II. New
857 thermobarometers, and practical assessment of existing thermobarometers. *Journal of*
858 *Petrology* 31, 1353–1378.

859 Bryndzia, L.T., Wood, B.J., 1990. Oxygen thermobarometry of abyssal spinel
860 peridotites; the redox state and C-O-H volatile composition of the Earth's sub-oceanic
861 upper mantle. *American Journal of Science* 290, 1093–1116.

862 Brüggmann, G., Batanova, V.G., Münker, C., Hofmann, A.W., 2002. Melt percolation
863 monitored by Os isotopes and HSE abundances : a case study from the mantle section
864 of the Troodos Ophiolite. *Earth and Planetary Science Letters* 204, 385–402.

865 Büchl, A., Brüggmann, G. E., Batanova, V. G., & Hofmann, A. W., 2004. Os
866 mobilization during melt percolation: The evolution of Os isotope heterogeneities in
867 the mantle sequence of the Troodos ophiolite, Cyprus. *Geochimica et Cosmochimica*
868 *Acta*, 68, 3397-3408.

869 Bulanova, G.P., Griffin, W.L., Ryan, C.G., Shestakova, O.Y., Barnes, S.-J., 1996. Trace
870 elements in sulfide inclusions from Yakutian diamonds. *Contributions to Mineralogy*
871 *and Petrology* 124, 111–125.

872 Cluzel, D., Aitchison, J.C., Picard, C., 2001. Tectonic accretion and underplating of
873 mafic terranes in the Late Eocene intraoceanic fore-arc of New Caledonia (Southwest
874 Pacific): geodynamic implications. *Tectonophysics* 340, 23–59.

875 Cluzel, D., Maurizot, P., Collot, J., Sevin, B., 2012. An outline of the Geology of New
876 Caledonia ; from Permian – Mesozoic Southeast Gondwanaland active margin to
877 Cenozoic obduction and supergene evolution. *Episodes* 35, 72–86.

878 Cluzel, D., Meffre, S., Maurizot, P., Crawford, A.J., 2006. Earliest Eocene (53 Ma)
879 convergence in the Southwest Pacific; evidence from pre- obduction dikes in the
880 ophiolite of New Caledonia. *Terra Nova* 18, 395–402.

881 Cluzel, D., Ulrich, M., Jourdan, F., Meffre, S., Paquette, J.L., Audet, M.A., Secchiari,
882 A., Maurizot, P., 2016. Early Eocene clinoenstatite boninite and boninite-series dikes
883 of the ophiolite of New Caledonia; a witness of slab-derived enrichment of the mantle
884 wedge in a nascent volcanic arc. *Lithos* 260, 429-442.

885 Cohen, A.S., Waters, F.G., 1996. Separation of osmium from geological materials by
886 solvent extraction for analysis by thermal ionisation mass spectrometry. *Analytica*
887 *Chimica Acta* 332, 269–275.

888 Dale, C.W., Burton, K.W., Pearson, D.G., Gannoun, A., Alard, O., Argles, T.W.,
889 Parkinson, I.J., 2009. Highly siderophile element behaviour accompanying subduction
890 of oceanic crust : Whole rock and mineral-scale insights from a high-pressure terrain.
891 *Geochimica et Cosmochimica Acta* 73, 1394–1416.

892 Debret, B., Andreani, M., Delacour, A., Rouméjon S., Trcera, N., EIMF, Williams, H.,
893 2017. E Assessing sulfur redox state and distribution in abyssal serpentinites using
894 XANES spectroscopy. *Earth and Planetary Science Letters* 466, 1–11.

895 Fischer-Gödde, M., Becker, H., Wombacher, F., 2011. Rhodium , gold and other highly
896 siderophile elements in orogenic peridotites and peridotite xenoliths. *Chemical*
897 *Geology* 280, 365–383.

898 Fonseca, R.O.C., Mallmann, G., St.C.O’Neill, H., Campbell, I.H., 2007. How chalcophile
899 is rhenium? An experimental study of the solubility of Re in sulphide mattes. *Earth*
900 *and Planetary Science Letters* 260, 537–548.

901 Fonseca, R.O.C., Mallmann, G., O'Neill, H.S., Campbell, I.H., Laurenz, V., 2011.
902 Solubility of Os and Ir in sulfide melt: Implications for Re/Os fractionation during
903 mantle melting. *Earth and Planetary Science Letters* 311, 339–350.

904 Fonseca, R.O.C., Laurenz, V., Mallmann, G., Luguet, A., Hoehne, N., Jochum, K.P.,
905 2012. New constraints on the genesis and long-term stability of Os-rich alloys in the
906 the Earth's mantle. *Geochimica et Cosmochimica Acta* 87, 227-242.

907 Goncharov, A. , 2018. In-situ iron oxidation state in the upper mantle minerals using
908 electron microprobe. Contributions to 3rd European mantle workshop. *Plinius* 44, p.
909 172. DOI:10.19276/plinius.2018.03015

910 Guo J., Griffin W. L., O'Reilly S. Y., 1999. Geochemistry and origin of sulphide
911 minerals in mantle xenoliths: Qilin, Southeastern China. *Journal of Petrology* 40,
912 1125–1149.

913 Harvey, J., Gannoun, A., Burton, K.W., Rogers, N.W., Alard, O., Parkinson, I.J., 2006
914 Ancient melt extraction from the oceanic upper mantle revealed by Re–Os isotopes in
915 abyssal peridotites from the Mid-Atlantic ridge. *Earth and Planetary Science Letters*
916 244, 606–621.

917 Hattori, K.H., Arai, S., Clarke Barrie, D.B., 2002. Selenium, tellurium, arsenic and
918 antimony contents of primary mantle sulfides. *Canadian Mineralogist* 40, 637–650.

919 Helmy, H.M., Ballhaus, C., Wohlgemuth-Ueberwasser, C., Fonseca, R.O.C., Laurenz,
920 V., 2010. Partitioning of Se, As, Sb, Te and Bi between monosulfide solid solution and
921 sulfide melt – Application to magmatic sulfide deposits. *Geochimica et Cosmochimica*
922 *Acta* 74, 6174–6179.

923 Höfer H. E., Brey G. P., 2007. The iron oxidation state of garnet by electron
924 microprobe: Its determination with the flank method combined with major-element
925 analysis. *American Mineralogist* 92, 873–885.

926 Kepezhinskas, P., Defant, M. J. and Widom, E., 2002. Abundance and distribution of
927 PGE and Au in the island-arc mantle: implications for sub-arc metasomatism. *Lithos*
928 60, 113–128.

929 Klein, F., Bach, W., 2009. Fe–Ni–Co–O–S Phase Relations in Peridotite–Seawater
930 Interactions. *Journal of Petrology* 50, 37–59.

931 Lagabrielle, Y., Chauvet, A., Ulrich, M., Guillot, S., 2013. Passive obduction and
932 gravity-driven emplacement of large ophiolitic sheets: The New Caledonia ophiolite
933 (SW Pacific) as a case study? *Bulletin de la Société Géologique de France* 184, 545–
934 556.

935 Lassiter, J.C., Byerly, B.L., Snow, J.E., Hellebrand, E., 2014. Constraints from Os-
936 isotope variations on the origin of Lena Trough abyssal peridotites and implications for
937 the composition and evolution of the depleted upper mantle. *Earth and Planetary*
938 *Science Letters* 403, 178–187.

939 Lee, C.T.A., Leeman, W.P., Canil, D., Li, Z.X.A., 2005. Similar V/Sc systematics in
940 MORB and arc basalts: Implications for the oxygen fugacities of their mantle source
941 regions. *Journal of Petrology* 46, 2313–2336.

942 Liu, C., Snow, J.E., Brügmann, G., Hellebrand, E., Hofmann, A.W., 2009. Non-
943 chondritic HSE budget in Earth 's upper mantle evidenced by abyssal peridotites from
944 Gakkel ridge (Arctic Ocean). *Earth and Planetary Science Letters* 283, 122–132.

945 Liu, J., Scott, J.M., Martin, C.E., Pearson, D.G., 2015. The longevity of Archean mantle
946 residues in the convecting upper mantle and their role in young continent formation.
947 Earth and Planetary Science Letters 424, 109–118.

948 Lorand, J.-P., 1991. Sulphide Petrology and Sulphur Geochemistry of Orogenic
949 Lherzolites: A Comparative Study of the Pyrenean Bodies (France) and the Lanzo
950 Massif (Italy). Journal of Petrology Special Volume, 77–95.

951 Lorand, J.-P., Pattou, L., Gros, M., 1999. Fractionation of Platinum-group Elements
952 and Gold in the Upper Mantle: a Detailed Study in Pyrenean Orogenic Lherzolites.
953 Journal of Petrology 40, 957–981.

954 Lorand, J., Luguët, A., Alard, O., 2008. Platinum-Group Elements : A New Set of Key
955 Tracers for the Earth's Interior. Elements 4, 247–252.

956 Lorand, J.P., Alard, O., 2010. Determination of selenium and tellurium concentrations
957 in Pyrenean peridotites (Ariege, France): New insight into S/Se/Te systematics of the
958 upper in mantle samples. Chemical Geology 278, 120–130.

959 Lorand, J.P., Alard, O., Luguët, A., Keays, R.R., 2003. Sulfur and selenium
960 systematics of the subcontinental lithospheric mantle: Inferences from the Massif
961 Central xenolith suite (France). Geochimica et Cosmochimica Acta 67, 4137–4151.

962 Lorand, J.P., Delpech, G., Grégoire, M., Moine, B., O'Reilly, S.Y., Cottin, J.Y., 2004.
963 Platinum-group elements and the multistage metasomatic history of Kerguelen
964 lithospheric mantle (South Indian Ocean). Chemical Geology 208, 195–215.

965 Luguët, A., Alard, O., Lorand, J.P., Pearson, N.J., Ryan, C.Y., Reilly, S.Y.O., 2001.
966 Laser-ablation microprobe (LAM) -ICPMS unravels the highly siderophile element
967 geochemistry of the oceanic mantle. Earth and Planetary Science Letters 189, 285–
968 294.

969 Luguët, A., Lorand, J.P., Seyler, M., 2003. Sulfide petrology and highly siderophile
970 element geochemistry of abyssal peridotites : A coupled study of samples from the
971 Kane Fracture Zone (45 ° W 23 ° 20N , MARK Area , Atlantic Ocean). *Geochimica et*
972 *Cosmochimica Acta* 67, 1553–1570.

973 Luguët, A., Lorand, J., Alard, O., Cottin, J., 2004. A multi-technique study of platinum
974 group element systematic in some Ligurian ophiolitic peridotites , Italy. *Chemical*
975 *Geology* 208, 175–194.

976 Luguët, A., Shirey, S.B., Lorand, J.P., Horan, M.F., Carlson, R.W., 2007. Residual
977 platinum-group minerals from highly depleted harzburgites of the Lherz massif
978 (France) and their role in HSE fractionation of the mantle. *Geochimica et*
979 *Cosmochimica Acta* 71, 3082–3097.

980 Marchesi, C., Garrido, C.J., Godard, M., Belley, F., Ferré, E., 2009. Migration and
981 accumulation of ultra-depleted subduction-related melts in the Massif du Sud ophiolite
982 (New Caledonia). *Chemical Geology* 266, 171–186.

983 Marchesi, C., Garrido, C.J., Harvey, J., 2013. Platinum-group elements , S , Se and Cu
984 in highly depleted abyssal peridotites from the Mid-Atlantic Ocean Ridge (ODP Hole
985 1274A): Influence of hydrothermal and magmatic processes. *Contributions to*
986 *Mineralogy and Petrology* 166, 1521–1538.

987 Mathez, E.A., 1976. Sulfur solubility and magmatic sulfides in submarine basalt glass.
988 *Journal of Geophysical Research* 81, 4269–4276.

989 McInnes, B. I. A., McBride, J. S., Evans, N. J., Lambert, D. D. & Andrew, A. S., 1999.
990 Osmium isotope constraints on ore metal recycling in subduction zones. *Science* 286,
991 512–516.

992 Meisel, T., Walker, R.J., Irving, A.J., Lorand, J.-P., 2001. Osmium isotopic
993 compositions of mantle xenoliths: a global perspective. *Geochimica et Cosmochimica*
994 *Acta* 65, 1311–1323.

995 Mungall J.E., Brenan, J., 2014. Partitioning of platinum-group elements and Au
996 between sulfide liquid and basalt and the origins of mantle-crust fractionation of the
997 chalcophile elements. *Geochimica et Cosmochimica Acta* 125, 265–289.

998 O’Driscoll, B., Day, J.M.D., Walker, R.J., Daly, J.S., McDonough, W.F., Piccoli, P.M.,
999 2012. Chemical heterogeneity in the upper mantle recorded by peridotites and
1000 chromitites from the Shetland Ophiolite Complex, Scotland. *Earth and Planetary*
1001 *Science Letters* 333–334, 226–237.

1002 Pagé, P., Barnes, S.-J., 2016. The influence of chromite on osmium, iridium,
1003 ruthenium and rhodium distribution during early magmatic processes. *Chemical*
1004 *Geology* 420, 51–68.

1005 Park, J., Campbell, I.H., Arculus, R.J., 2013. Platinum-alloy and sulfur saturation in an
1006 arc-related basalt to rhyolite suite : Evidence from the Pual Ridge lavas , the Eastern
1007 Manus Basin. *Geochimica et Cosmochimica Acta* 101, 76–95.

1008 Pearson, D.G., Irvine, G.J., Ionov, D.A., Boyd, F.R., Dreibus, G.E., 2004. Re-Os
1009 isotope systematics and platinum group element fractionation during mantle melt
1010 extraction: A study of massif and xenolith peridotite suites. *Chemical Geology* 208,
1011 29–59.

1012 Pirard, C., Hermann, J., O’Neill, H.St.C., 2013. Petrology and geochemistry of the
1013 crust– mantle boundary in a nascent arc, Massif du Sud ophiolite, New Caledonia, SW
1014 Pacific. *Journal of Petrology* 0, 1–34.

1015 Rehkämper, M., Halliday, A.N., Alt, J., Fitton, J.G., Zipfel, J., Takazawa, E., 1999.
1016 Non-chondritic platinum-group element ratios in oceanic mantle lithosphere:
1017 petrogenetic signature of melt percolation? *Earth and Planetary Science Letters* 172,
1018 65–81.

1019 Reisberg, L., Lorand, J.-P., 1995. Longevity of sub-continental mantle lithosphere
1020 from osmium isotope systematics in orogenic peridotite massifs. *Nature* 376, 159–
1021 162.

1022 Saha, A., Basu, A.R., Jacobsen, S.B., Poreda, R.J., 2005. Slab devolatilization and Os
1023 and Pb mobility in the mantle wedge of the Kamchatka arc. *Earth and Planetary
1024 Science Letters* 236, 182–194.

1025 Salters, V.J.M., Stracke, A., 2004. Composition of the depleted mantle. *Geochemistry
1026 Geophysics Geosystems* 5 (5).

1027 Scott, J.M., Liu, J., Pearson, D.G., Harris, G.A., Czertowicz, T.A., Woodland, S.J.,
1028 Riches, A.J.V., Luth, R.W., 2019. Continent stabilisation by lateral accretion of
1029 subduction zone-processed depleted mantle residues; insights from Zealandia. *Earth
1030 and Planetary Science Letters* 507, 175–186.

1031 Scott, J.M., Liu, J., Pearson, D.G., Waight, T.E., 2016. Mantle depletion and
1032 metasomatism recorded in orthopyroxene in highly depleted peridotites. *Chemical
1033 Geology* 441, 280–291.

1034 Secchiari, A., Montanini, A., Bosch, D., Macera, P., Cluzel, D., 2019a. Sr-Nd-Pb and
1035 trace element systematics of the New Caledonia harzburgites: tracking source
1036 depletion and contamination processes in a SSZ setting. In press on *Geoscience
1037 Frontiers*, special issue Ophiolites

1038 Secchiari, A., Montanini, A., Bosch, D., Macera, P., Cluzel, D., 2019b. Origin of the
1039 spinel-pyroxene symplectites in the harzburgites from the New Caledonia peridotite.
1040 *Ophioliti* 44, 31-42.

1041 Secchiari, A., Montanini, A., Bosch, D., Macera, P., Cluzel, D., 2018. The contrasting
1042 geochemical message from the New Caledonia gabbro-norites: insights on depletion
1043 and contamination processes of the sub-arc mantle in a nascent arc setting.
1044 *Contributions to Mineralogy and Petrology* 173, 66.

1045 Secchiari, A., Montanini, A., Bosch, D., Macera, P., Cluzel, D., 2016. Melt extraction
1046 and enrichment processes in the New Caledonia lherzolites: evidence from
1047 geochemical and Sr–Nd isotope data. *Lithos* 260, 28–43.

1048 Secchiari, A., 2016. Sr-Nd-Pb isotope investigation of the New Caledonia Ophiolite.
1049 PhD thesis, Parma and Montpellier University, 191 pp.

1050 Snow, J.E., Reisberg, L., 1995. Os isotopic systematics of the MORB mantle: results
1051 from altered abyssal peridotites. *Earth and Planetary Science Letters* 133, 411–421.

1052 Snow, J., Schmidt, G., Rampone E., 2000. Os isotopes and highly siderophile
1053 elements (HSE) in the Ligurian ophiolites, Italy. *Earth and Planetary Science Letters*
1054 175, 119-132

1055 Standish, J.J., Hart, S.R., Blusztajn, J., Dick, H.J.B., Lee, K.L., 2002. Abyssal
1056 peridotite osmium isotopic compositions from Cr-spinel. *Geochemistry Geophysics*
1057 *Geosystems* 3, (1).

1058 Ulmer, P., 2001. Partial melting in the mantle wedge — the role of H₂O in the genesis
1059 of mantle-derived 'arc-related' magmas. *Physics of the Earth and Planetary Interiors*
1060 127, 215–232.

1061 Ulrich, M., Picard, C., Guillot, S., Chauvel, C., Cluzel, D., Meffre, S., 2010. Multiple
1062 melting stages and refertilization as indicators for ridge to subduction formation: the
1063 New Caledonia ophiolite. *Lithos* 115, 223–236.

1064 Walker, R.J., Hanski, E., Vuollo, J., Liipo, J., 1996. The Os isotopic composition of
1065 Proterozoic upper mantle: evidence for chondritic upper mantle from the Outokumpu
1066 ophiolite, Finland. *Earth and Planetary Science Letters* 141, 161–173.

1067 Wang, Z., Becker, H., 2013. Ratios of S, Se and Te in the silicate Earth require a
1068 volatile-rich late veneer. *Nature* 499, 328–331.

1069 Wang, Z., Becker, H., Gawronski, T., 2013. Partial re-equilibration of highly
1070 siderophile elements and the chalcogens in the mantle : A case study on the
1071 Baldissero and Balmuccia. *Geochimica et Cosmochimica Acta* 108, 21–44.

1072 Whattam, S. A., 2009. Arc-continent collisional orogenesis in the SW Pacific and the
1073 nature, source and correlation of emplaced ophiolitic nappe components. *Lithos* 113,
1074 88–114.

1075 Widom, E., Kepezhinskas, P., and Defant, M., 2003, The nature of metasomatism in
1076 the sub-arc mantle wedge: Evidence from Re-Os isotopes in Kamchatka peridotite
1077 xenoliths: *Chemical Geology* 196, 283–306.

1078 Widom, E., 2011. Recognizing recycled Osmium. *Geology* 39, 1087–1088.

1079

1080 Figure captions

1081 Fig. 1. a) Present-day structures of the Southwest Pacific region modified after Cluzel
1082 et al. (2012). Dark orange, land; light orange, continental plateau; white, oceanic
1083 basins (LHR: Lord Howe Rise, NR: Norfolk ridge, LR: Loyalty ridge, HP: Hikurangi

1084 Plateau); b) simplified geological map of New Caledonia showing distribution of the
1085 Peridotite massifs (modified after Cluzel et al., 2012).

1086

1087 Fig. 2. Variations of Os, Ru, Rh, Pt, Pd, Au and Re vs. Ir for the New Caledonia
1088 peridotites. Abyssal peridotites (Kane fracture zone: Snow and Schmidt, 1998;
1089 Brandon et al., 2000; Luguet et al., 2001, 2003; Marchesi et al., 2013; MAR: Harvey
1090 et al., 2006; Lena trough: Lassiter et al., 2014) and ophiolitic peridotites (IL-EL:
1091 Internal and External Ligurides, Snow et al., 2000; Luguet et al., 2004; Fischer-Godde
1092 et al., 2011; Lanzo: Becker et al., 2006; Pyrenees: Becker et al., 2006; Luguet et al.,
1093 2007) are shown for comparison.

1094

1095 Fig. 3. Primitive mantle normalised HSE and chalcogen patterns for the New Caledonia
1096 spinel and plagioclase lherzolites. Grey shaded area includes oceanic lherzolites from
1097 Mid-Atlantic and South West Indian ridges (Snow and Schmidt, 1998; Luguet et al.,
1098 2001; Luguet et al., 2003) and ophiolitic lherzolites from the Ligurian Units (Snow et
1099 al., 2000; Luguet et al., 2004; Fischer-Gödde et al. 2011). Normalising values after
1100 Becker et al. (2006), Fischer-Gödde et al. (2011) and Wang and Becker (2013).

1101

1102 Fig. 4. a) Al_2O_3 (wt.%) - $^{187}\text{Os}/^{188}\text{Os}_i$ and b) Os - $^{187}\text{Os}/^{188}\text{Os}_i$ and c) $^{187}\text{Re}/^{188}\text{Os}$ -
1103 $^{187}\text{Os}/^{188}\text{Os}$ diagrams showing data from New Caledonia lherzolites and type-A
1104 harzburgites in comparison to PM compositions. PM data from Meisel et al. (1996).
1105 Data for abyssal peridotites are from Harvey et al., (2006) for Atlantic peridotites,
1106 Lassiter et al., (2014) for Lena through and Liu et al. (2015) for Gakkel ridge. See Fig.
1107 2 for ophiolitic peridotites references.

1108

1109 Fig. 5. a) Te vs. Se, b) Te vs. Pd and c) S vs. S/Se correlation diagrams for New
1110 Caledonia spinel and plagioclase Iherzolites. Also showing for comparison data for
1111 orogenic Iherzolites from Wang and Becker (2013).

1112

1113 Fig. 6. a) Primitive mantle normalised HSE and chalcogen abundances in type-A
1114 harzburgites. Light grey shaded field encompasses the area of modern MOR
1115 harzburgites (Snow and Schmidt, 1998; Lugué et al., 2001, 2003; Harvey et al.,
1116 2006; Marchesi et al., 2013); b) Primitive mantle normalised diagram showing HSE
1117 and chalcogen patterns of type-B harzburgites. Normalising values are after Becker et
1118 al. (2006), Fischer-Gödde et al. (2011) and Wang and Becker (2013).

1119

1120 Fig. 7. Primitive mantle normalised HSE abundances of a) type-A and b) type-B
1121 harzburgites compared to the HSE composition displayed by New Zealand mantle
1122 xenoliths. See text for further detail.

1123

Figure 1
[Click here to download high resolution image](#)

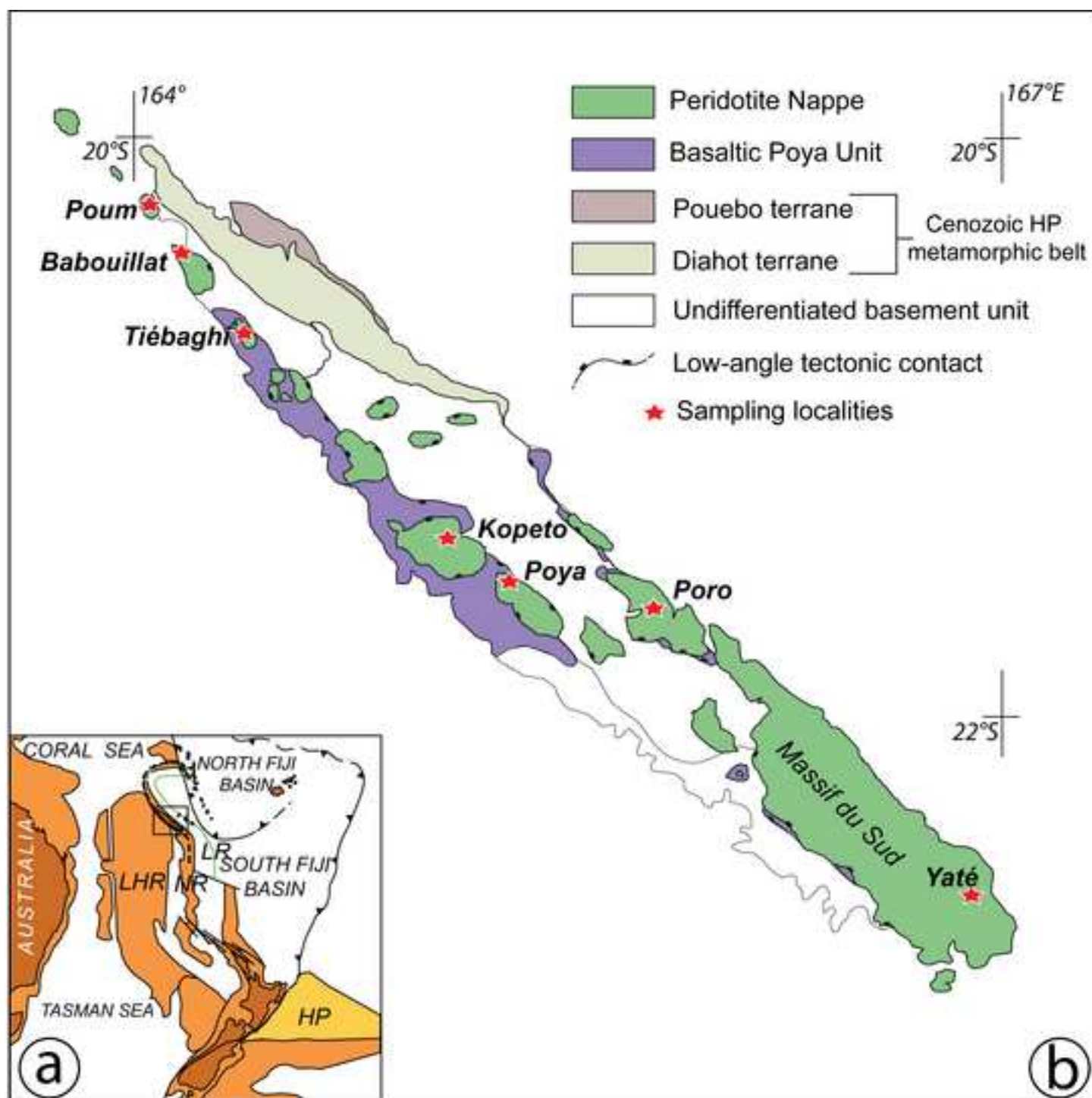


Figure 2

[Click here to download high resolution image](#)

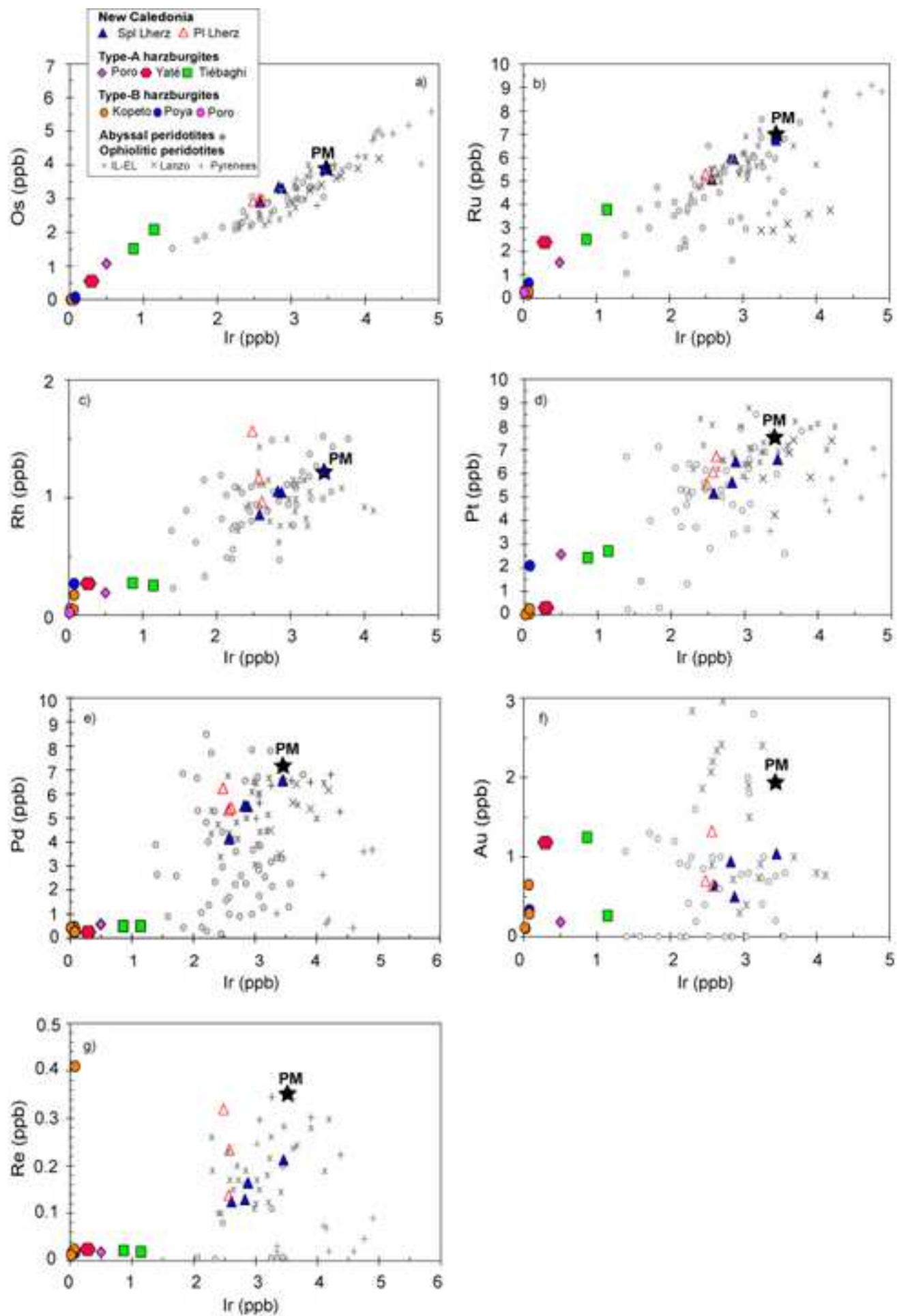


Figure 3
[Click here to download high resolution image](#)

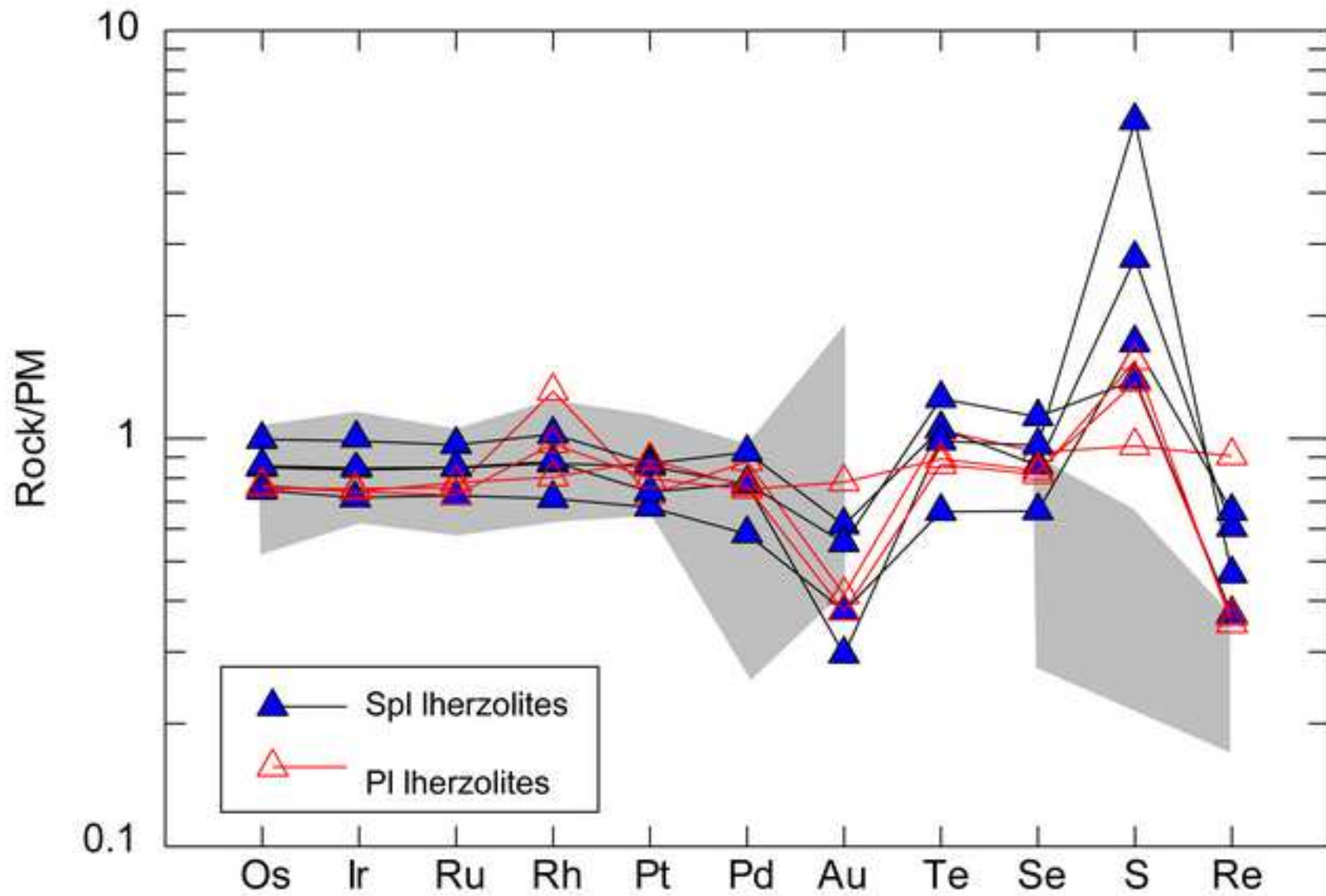


Figure 4

[Click here to download high resolution image](#)

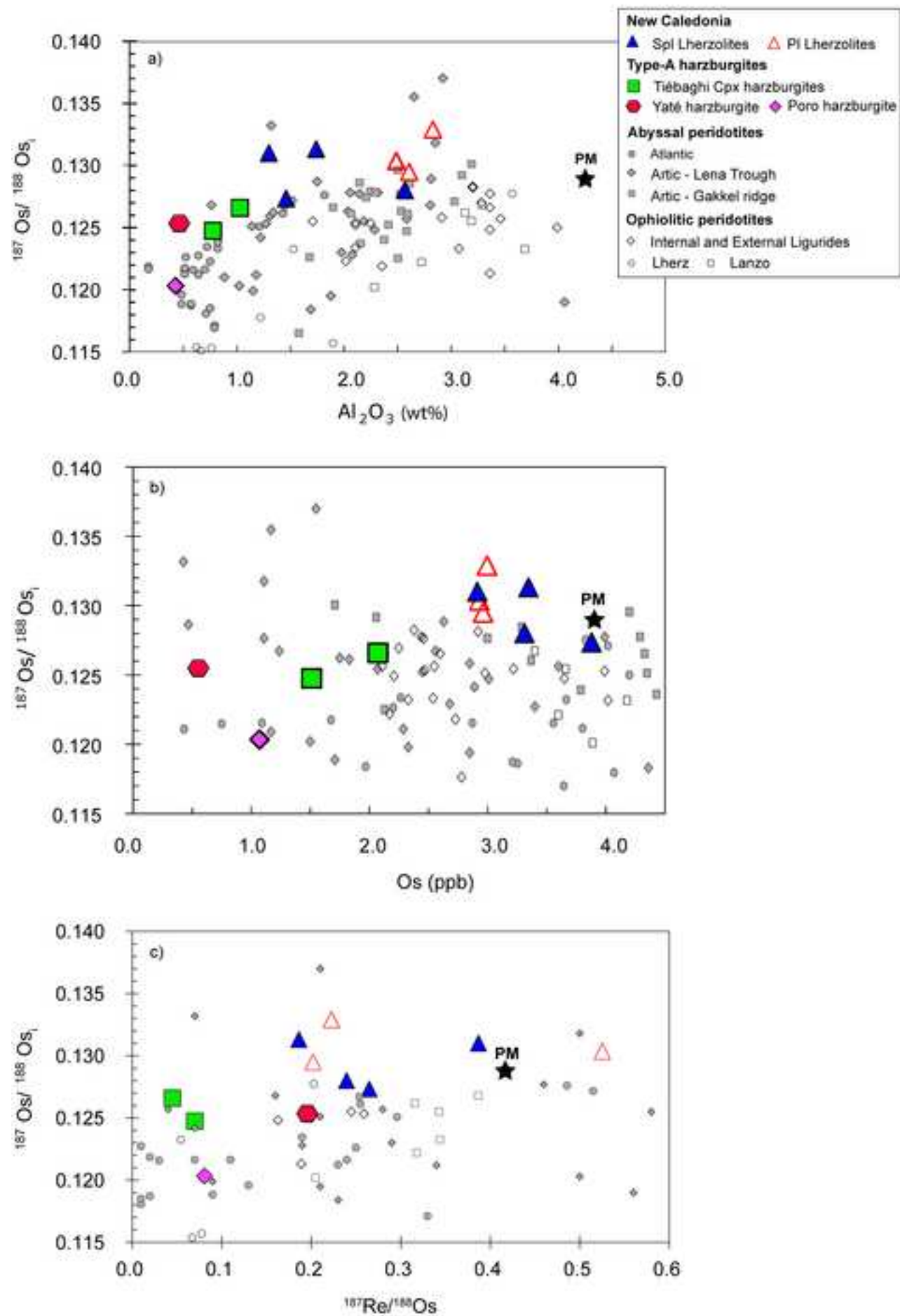


Figure 5

[Click here to download high resolution image](#)

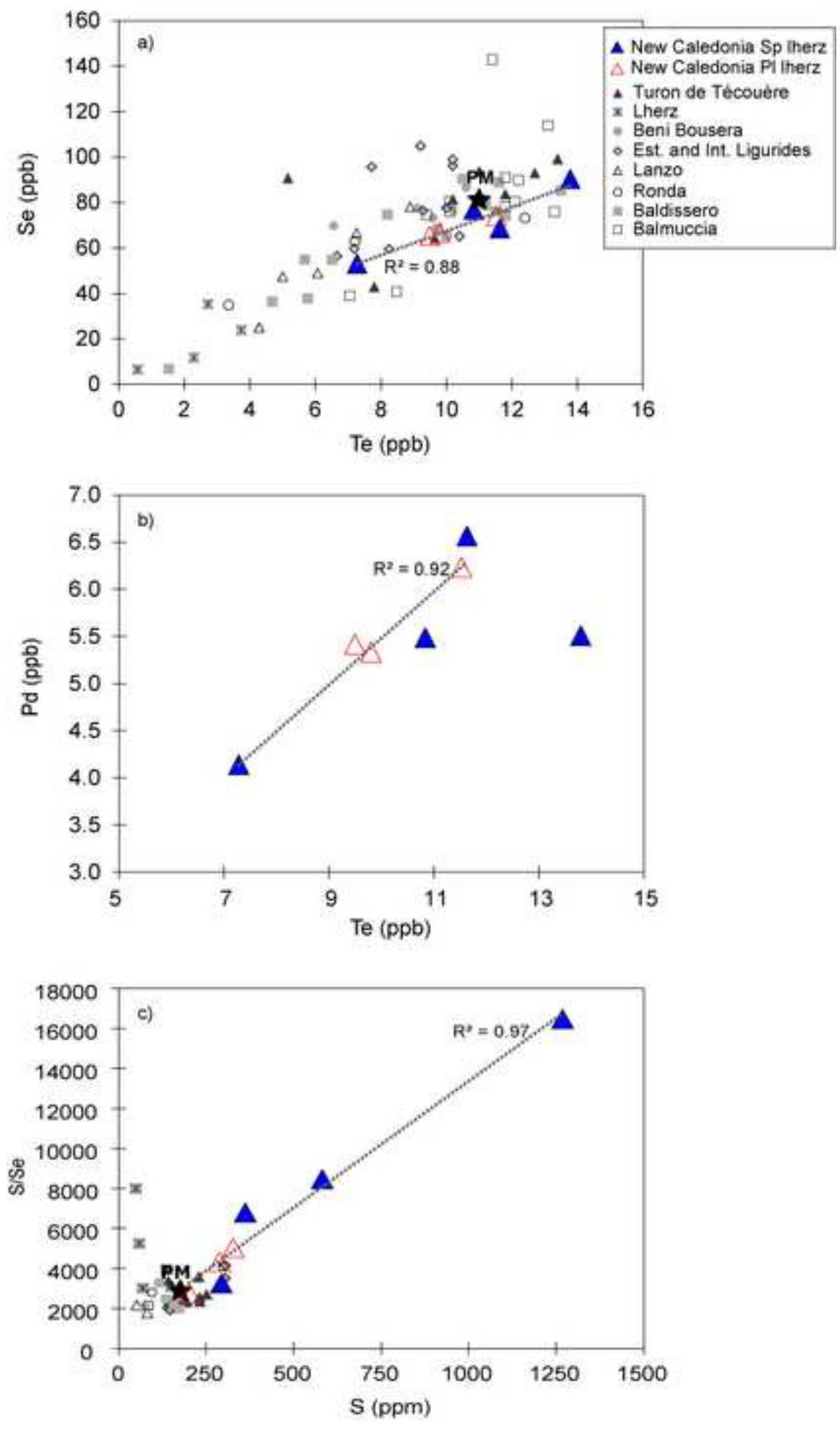


Figure 6
[Click here to download high resolution image](#)

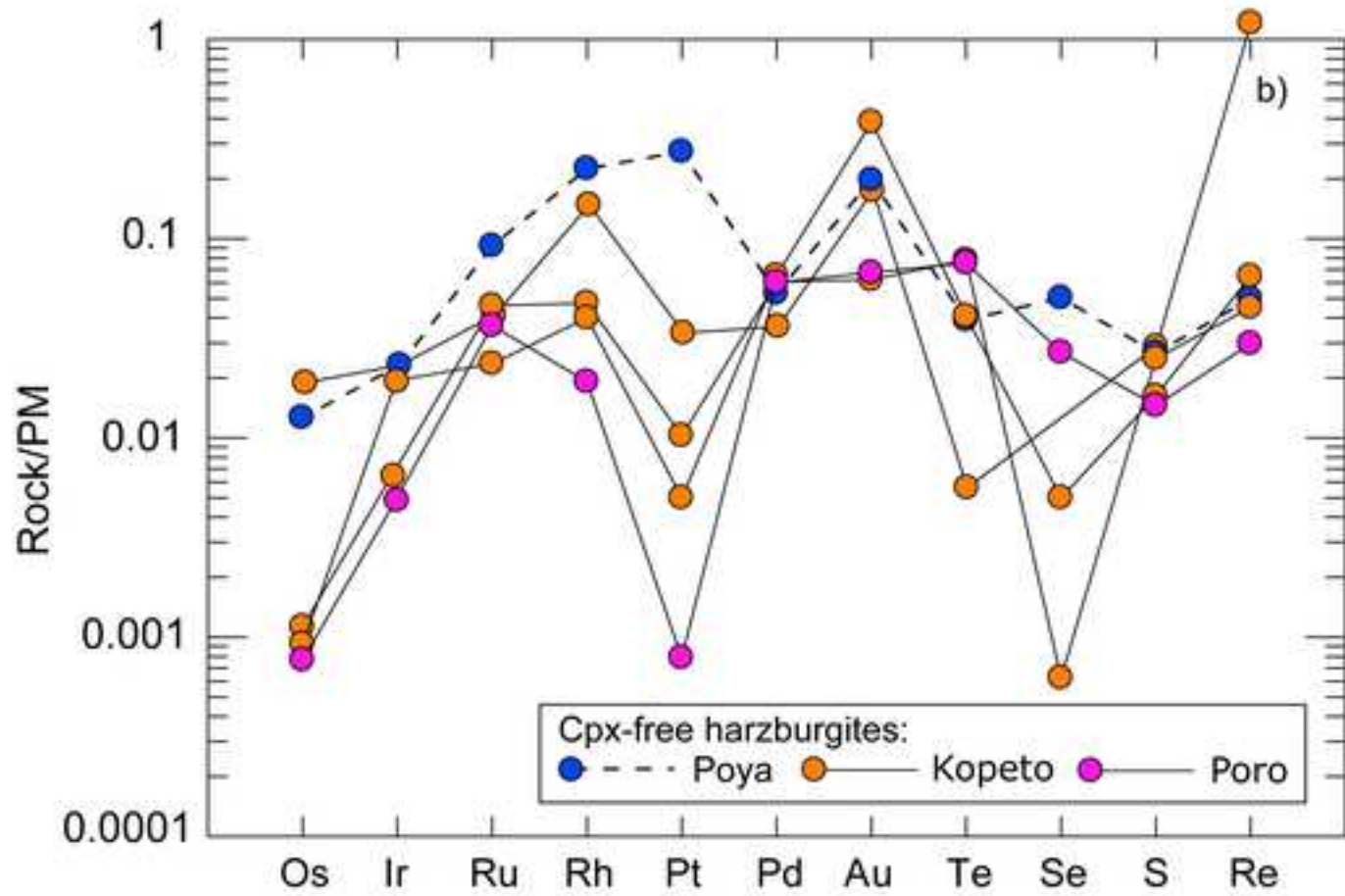
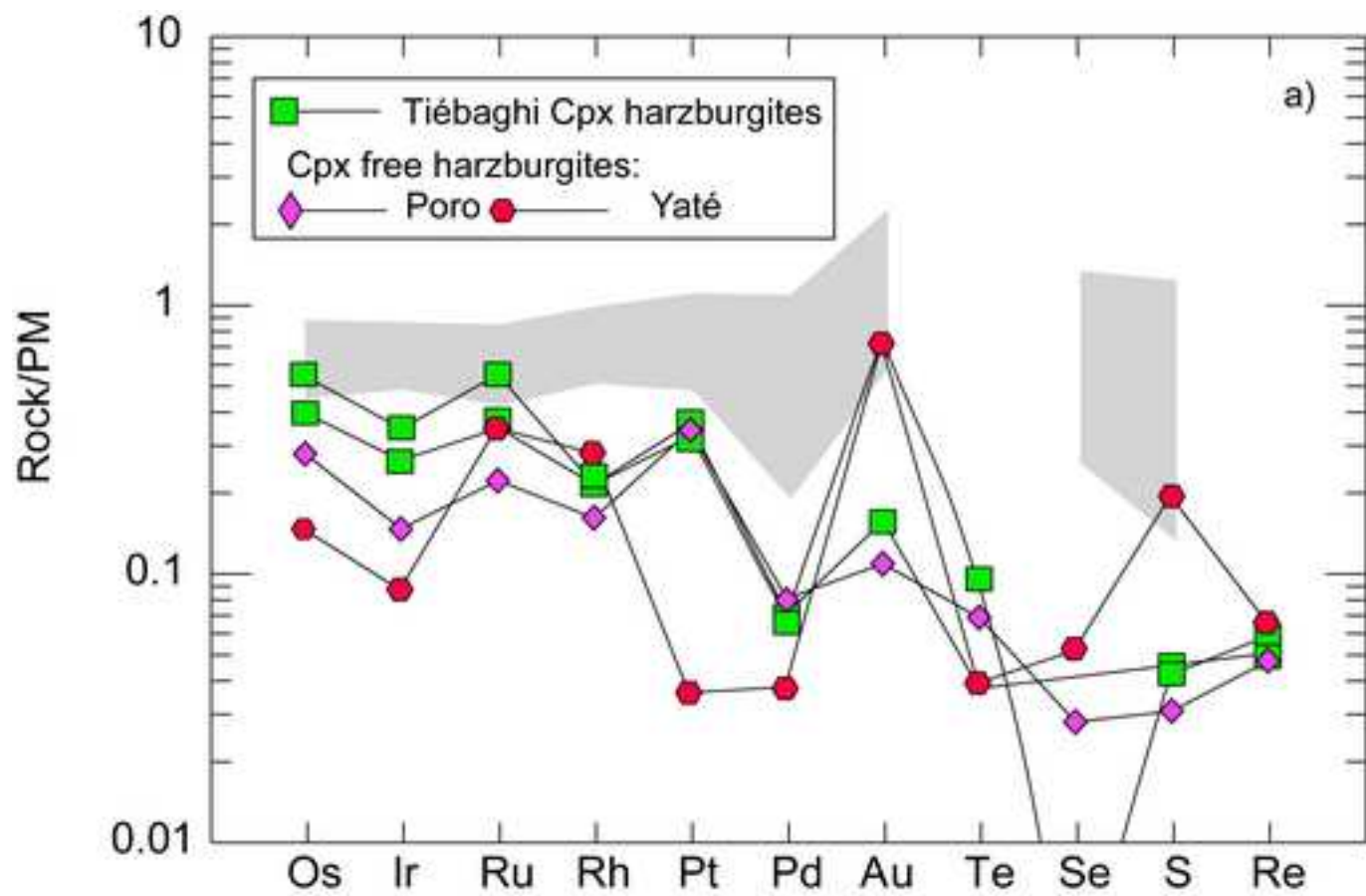
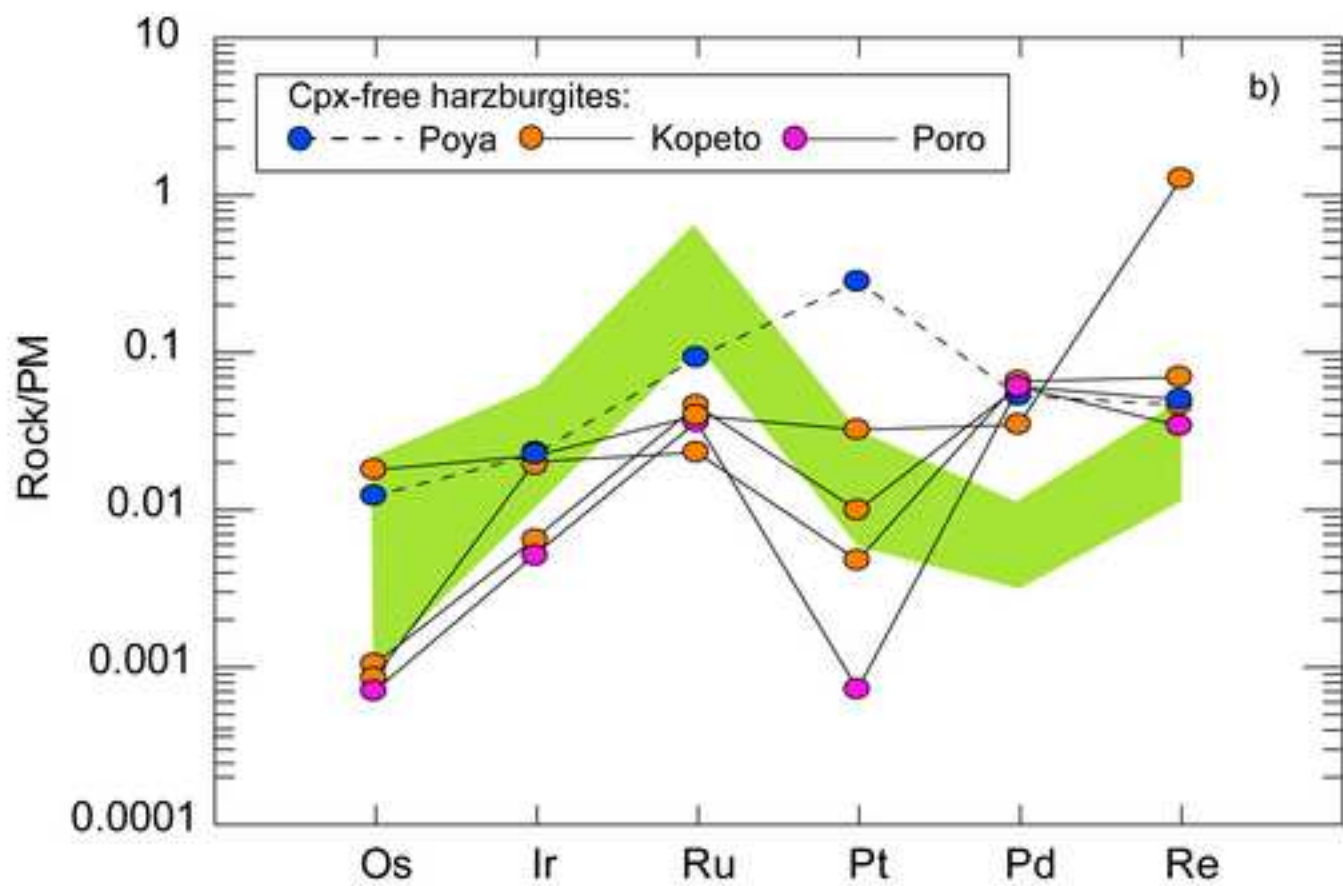
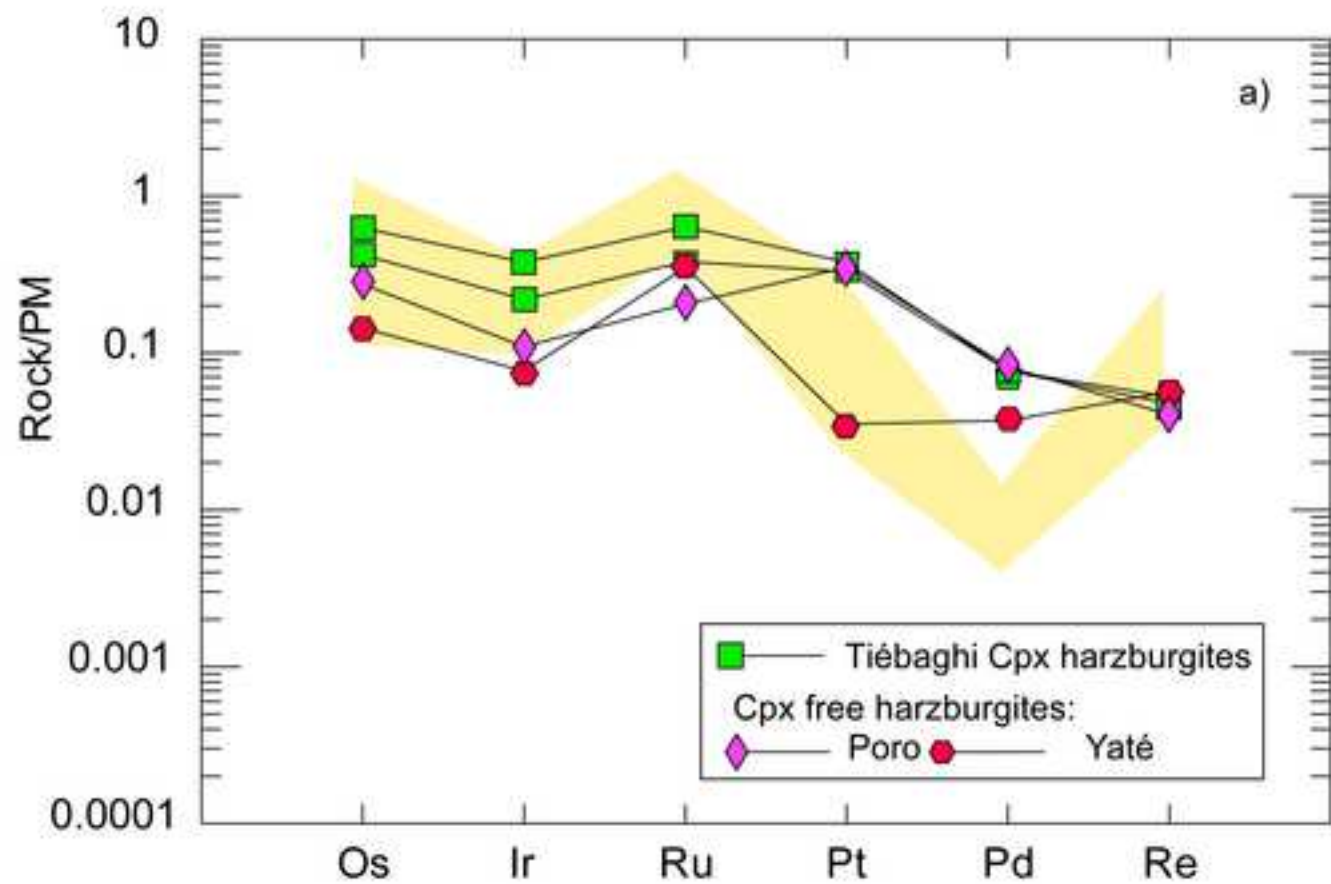
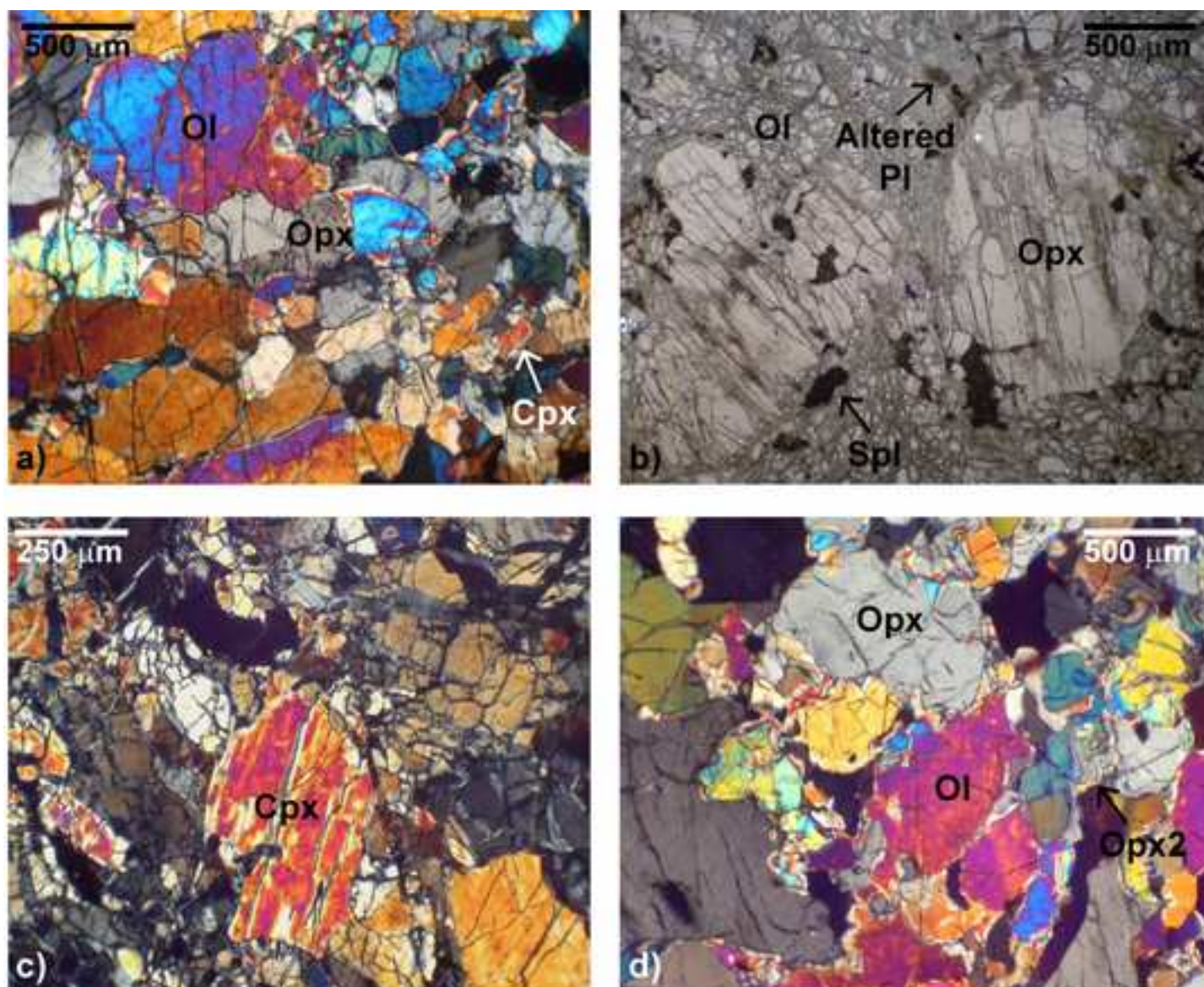
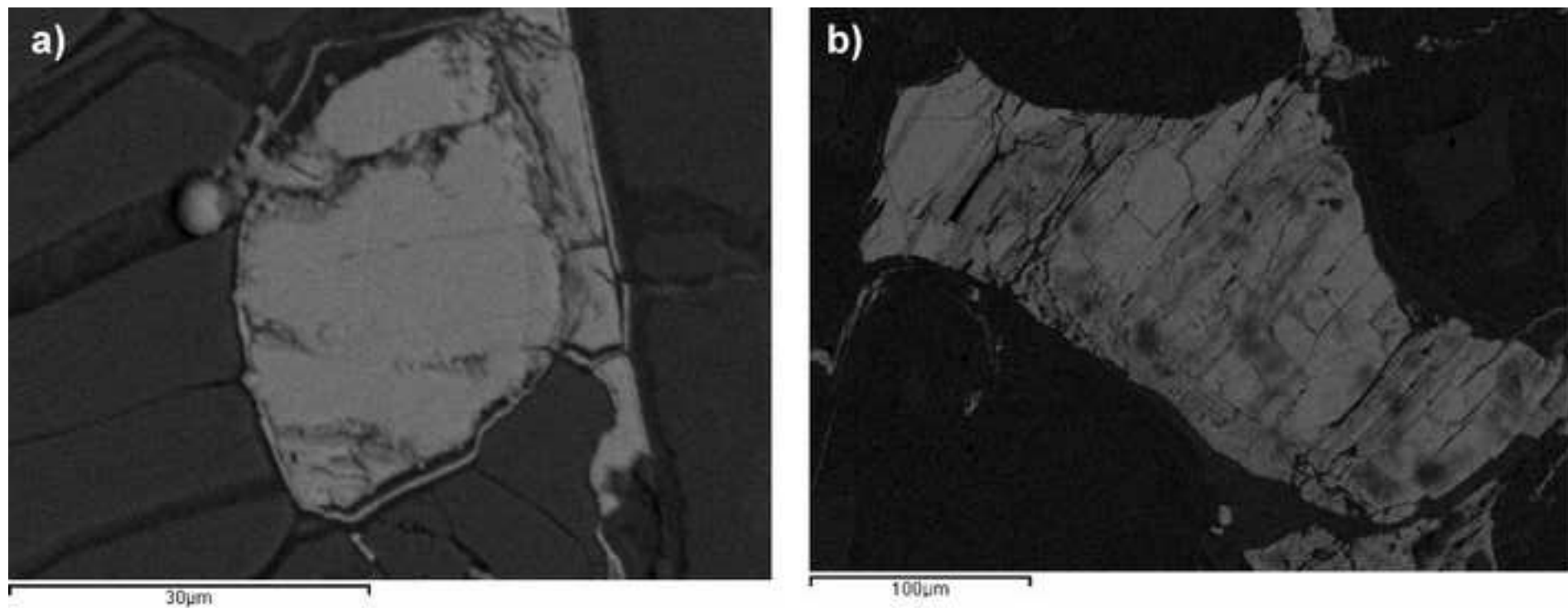


Figure 7
[Click here to download high resolution image](#)





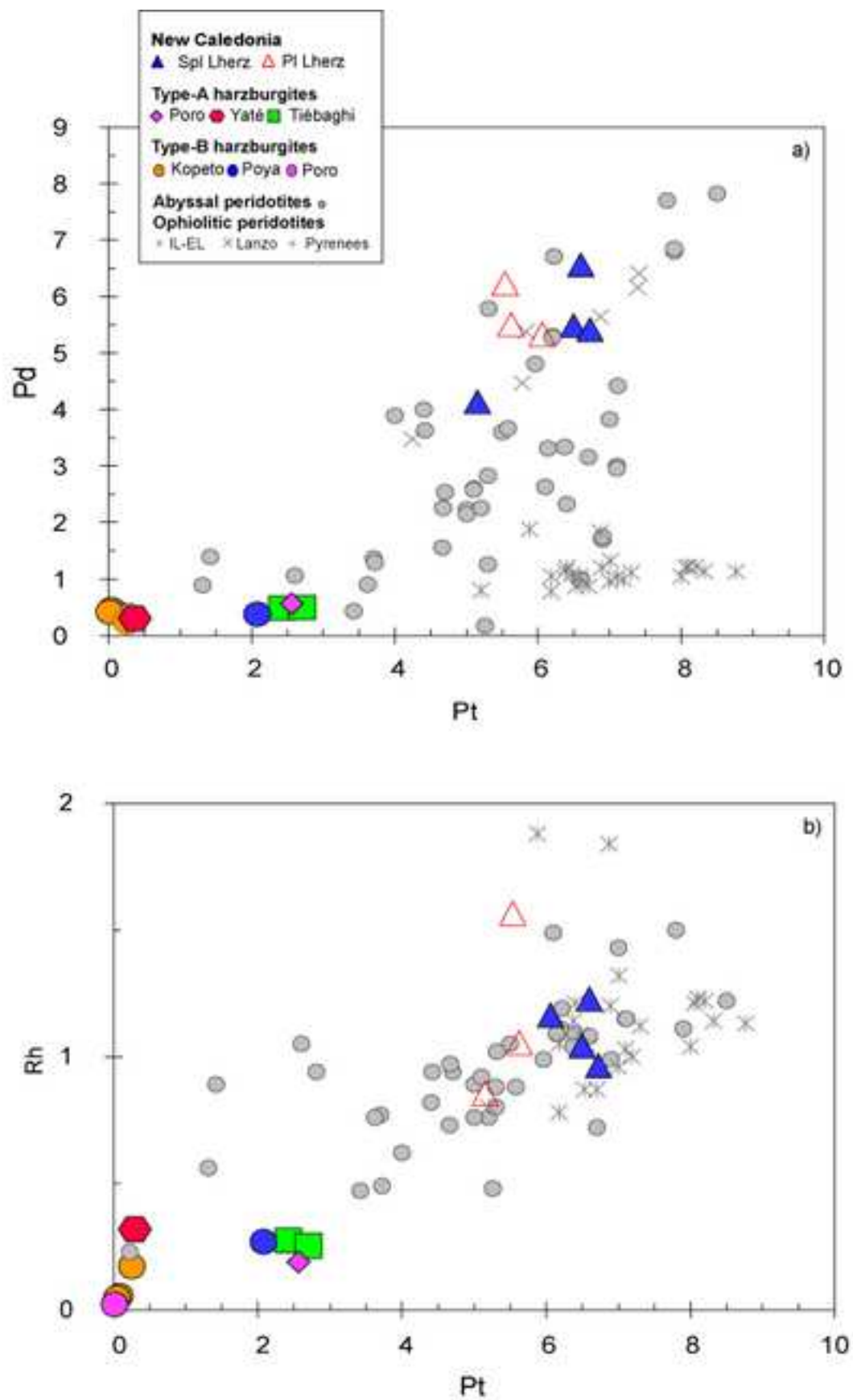
Microphotographs of the New Caledonia peridotites: a) porphyroclastic texture marked by deformed and stretched olivine and orthopyroxene crystals in spl-lherzolite POU2; b) plagioclase-lherzolite thin section (BAB2A, parallel polars); c) strongly exsolved, primary clinopyroxene occurrence in T12 harzburgite; d) interstitial orthopyroxene (opx2) formed at the expense of primary olivine (KPT5 harzburgite).



BSE images of sulphides in the New Caledonia Iherzolites: a) small included sulphide (BA1); b) larger intergranular sulphide in POU2 Iherzolite.

Figure S3

[Click here to download high resolution image](#)



Pt vs. a) Pd and b) Rh variation diagrams for the New Caledonia peridotites. Abundances are in ppb.

Table 1
[Click here to download Table: Table 1.xlsx](#)

Table 1
 Concentrations of the HSE, S, Se and Te, Os isotopes, selected major elements and ratios for the New Caledonia peridotites

Sample	Rock	Al ₂ O ₃ wt.%	LOI %	Os (ng/g)	Ir (ng/g)	Ru (ng/g)	Rh (ng/g)	Pt (ng/g)	Pd (ng/g)	Au (ng/g)	Re (ng/g)	Os _N /Ir _N	Os _N /Ru _N	Pd _N /Ir _N	Ru _N /Ir _N	Pt _N /Ir _N	Pt _N /Ru _N	¹⁸⁷ Re/ ¹⁸⁸ Os (2SE)	¹⁸⁷ Os/ ¹⁸⁸ Os measured	2SE	¹⁸⁷ Os/ ¹⁸⁸ Os _i	γOs _(33Ma)	T _{MA} (PM) Ga	T _{RD} (PM) Ga	T _{RD2} (PM) Ga	S (μg/g)	Se (ng/g)	Te (ng/g)	S/Se	Se/Te		
POU1A	PI L	2.49	7.56	2.93	2.48	5.31	1.57	5.54	6.23	0.704	0.319	1.06	0.99	1.24	1.07	1.03	0.96	0.525(1)	0.130822	9.1E-06	0.130358	2.9	0.8	f	f	202	74.9	11.5	2703	6.5		
POU2	Sp L	1.46	8.63	3.88	3.45	6.76	1.23	6.60	6.56	1.04	0.213	1.01	0.18	0.94	5.71	0.88	0.15	0.265(1)	0.127574	6.8E-06	0.127340	0.5	0.7	f	0.3	582	69.6	11.6	8364	6.0		
POU2B	Sp L	2.57	10.69	3.31	2.88	5.93	1.04	6.49	5.49	0.503	0.165	1.03	1.09	0.94	0.95	1.04	1.09	0.240(1)	0.128227	8.0E-06	0.128016	1.1	0.4	f	0.2	1268	77.8	10.8	16289	7.2		
POU3	Sp L	1.30	9.60	2.91	2.58	5.07	0.86	5.15	4.14	0.642	0.234	1.01	1.05	0.79	0.97	0.92	0.95	0.387(1)	0.131356	9.1E-06	0.131015	3.4	f	f	f	362	54.0	7.3	6691	7.4		
BA1	Sp L	1.74	6.39	3.34	2.85	5.95	1.05	5.62	5.51	0.943	0.129	1.06	0.27	0.96	3.88	0.92	0.24	0.186(1)	0.131485	7.9E-06	0.131320	3.7	f	f	f	294	91.3	13.8	3218	6.6		
BAB1B	PI L	2.61	6.98	2.96	2.61	5.46	0.965	6.73	5.42	0.641	0.125	1.02	0.24	1.02	4.30	1.19	0.28	0.202(1)	0.129664	8.9E-06	0.129485	2.2	f	f	0.0	327	66.2	9.5	4943	7.0		
BAB2B	PI L	2.83	8.43	3.00	2.57	5.08	1.16	6.06	5.33	1.33	0.138	1.05	1.67	1.02	0.63	1.09	1.73	0.223(1)	0.133084	8.9E-06	0.132887	4.9	f	f	f	289	67.6	9.8	4278	6.9		
TI1	H	0.78	9.01	1.51	0.864	2.52	0.275	2.42	0.488	1.25	0.022	1.57	1.08	0.28	1.46	1.29	0.89	0.070(25)	0.12479	1.7E-05	0.12473	-1.5	0.8	0.7	0.7	9	1.1	1.0	8188	1.0		
TI2	H	1.03	6.04	2.07	1.14	3.78	0.254	2.70	0.499	0.264	0.019	1.63	0.98	0.21	1.65	1.09	0.66	0.045(18)	0.12662	1.3E-05	0.12658	-0.1	0.5	0.4	0.4	10	0.7	0.4	14053	1.7		
PO4	H	0.43	0.18	1.07	0.499	1.53	0.191	2.56	0.570	0.160	0.018	1.93	1.26	0.56	1.53	2.36	1.54	0.081(35)	0.12040	2.4E-05	0.12033	-5.0	1.5	1.3	1.3	6	3.1	0.8	2084	4.1		
YA1	H	0.46	6.83	0.554	0.297	2.35	0.326	0.268	0.263	1.17	0.022	1.67	0.42	0.44	3.95	0.42	0.11	0.196(68)	0.12551	4.7E-05	0.12534	-1.0	1.0	0.6	0.6	40	4.9	0.4	8117	11.4		
PY1	H	0.78	0.00	0.049	0.077	0.643	0.269	2.08	0.378	0.336	0.016	0.58	0.14	2.43	4.19	2.97	2.97	1.62(8)	0.1299	5.3E-04	0.1284	1.4	0.0	0.0	0.2	6	0.9	0.9	6103	1.1		
Duplicate				0.023	0.133	0.693	0.171	2.44	0.588	0.311	0.062							13.0(1)	0.127	1.0E-03	0.115	-8.9				53	0.3	1.0	196197	0.3		
KPT2	H	0.70	3.03	0.004	0.022	0.323	0.057	0.078	0.431	0.107	0.018	0.18	0.02	9.50	7.22	0.22	0.22	19(1)	0.148	5.6E-03	0.131	3.6	0.1	f	f	5	1.3	0.4	4164	2.8		
Duplicate				0.036	0.017	0.211	0.040	0.210	0.620	0.144	0.010							1.4(1)	0.302	1.3E-03	0.301	137.8				7	1.3	8.2	4947	0.2		
KPT5	H	0.74	0.12	0.004	0.066	0.165	0.048	0.038	0.464	0.654	0.024	0.05	0.04	3.46	1.25	0.21	0.21	32(2)	0.147	6.2E-03	0.118	-6.6	0.0	f	f	3	3.0	0.7	1133	4.1		
Duplicate				0.007	0.062	0.165	0.054	0.046	0.512	0.603	0.056							37(1)	0.160	3.2E-03	0.127	0.5				3	0.7	1.3	4453	0.5		
PO3	H	0.41	0.00	0.003	0.015	0.256	0.023	0.006	0.428	0.084	0.012	0.18	0.02	14.12	8.57	0.02	0.02	19(2)	0.153	8.4E-03	0.136	8.0	0.1	f	f	3	1.4	0.6	2129	2.2		
Duplicate				0.055	0.018	0.243	0.016	0.009	0.573	0.293	0.0078							0.69(7)	0.1239	4.7E-04	0.1233					bdl	bdl	0.8	-	-	-	-
KPT3	H	0.67	0.67	0.072	0.079	0.280	0.172	0.248	0.250	0.288	0.410	0.81	1.87	0.17	0.19	6.92	6.92	28(1)	0.1273	3.5E-04	0.1204	-5.1	0.0	0.3	1.3	6	bdl	bdl	-	-	-	-

Duplicate: replicate digestion of the same sample powder
¹L= plagioclase lherzolite, Sp L= spinel lherzolite, H= harzburgite
 Values of PM ¹⁸⁷Os/¹⁸⁸Os = 0.1296 and ¹⁸⁷Re/¹⁸⁸Os = 0.434 used for calculation of T_{MA} and T_{RD} ages (Meisel et al., 2001); f= future model ages. T_{RD2}(PM) indicates depletion ages calculated taking into account Re addition that may have occurred during peridotite evolution.

Table 2[Click here to download Table: Table 2.xlsx](#)**Table 2**

Equilibration Temperature, Pressure, and Oxygen Fugacity Calculated for selected peridotite samples

Sample	Type	T BK (°C)	P (GPa)	Wood (1990)		T Ol-Spl (°C)	Wood (1990)	
				log $f(O_2)$	Δ FMQ		log $f(O_2)$	Δ FMQ
TI2	Type-A harz	930	1.5	-10.40	0.71	870	-11.37	0.76
YA1	Type-A harz	980	1.5	-9.83	0.50	815	-12.66	0.50
KPT5	Type-B harz	1130	1.5	-7.91	0.39	840	-12.20	0.48
PO3A	Type-B harz	1000	1.5	-9.86	0.17	940	-10.76	0.18
PY1B	Type-B harz	1050	1.5	-9.17	0.16	930	-10.90	0.20
BA1	Spl lherz	1060	1.5	-13.1503	-3.96	880	-15.66	-3.73

T BK= Equilibration temperature calculated on Opx porphyroclasts using Brey and Köhler (1990)

T Ol-Spl = Equilibration temperature calculated using Li et al. (1995) formulation

Oxygen fugacity estimates are from Wood et al. (1990) and are reported as Δ log fO_2 from the quartz-fayalite-magnetite (FMQ) buffer using the $Fe^{3+}/\Sigma Fe$ values of the analysed spinels. See text for further details.

Table S1[Click here to download Table: Table S1.xlsx](#)**Table S1**

Major element composition for selected sulphides from the New Caledonia lherzolites

Sample	POU2	POU2	POU2	POU2	POU2	POU2	POU2	BA1	BA1	BA1	BA1	BA1
Mineral	<i>mss</i>	<i>mss</i>	<i>mss</i>	<i>pn</i>	<i>pn</i>	<i>pn</i>	<i>pn</i>	<i>mss</i>	<i>mss</i>	<i>mss</i>	<i>mss</i>	<i>mss</i>
Occurrence	<i>Intergr</i>	<i>Intergr</i>	<i>Incl</i>	<i>Incl</i>	<i>Incl</i>	<i>Incl</i>	<i>Incl</i>	<i>Incl</i>	<i>Incl</i>	<i>Incl</i>	<i>Incl</i>	<i>Incl</i>
<i>wt%</i>	<i>p</i>	<i>p</i>	<i>p</i>	<i>p</i>	<i>p</i>	<i>p</i>	<i>p</i>	<i>p</i>	<i>p</i>	<i>p</i>	<i>p</i>	<i>p</i>
S	34.32	34.39	32.74	33.24	41.19	32.68	40.82	33.22	33.08	32.47	32.53	33.13
Fe	41.23	43.80	36.65	28.09	23.90	29.14	24.68	36.85	42.99	43.25	42.19	43.02
Co	0.64	0.59	0.78	0.46	1.93	1.91	2.26	0.46	0.50	0.55	0.80	0.58
Ni	23.28	20.44	29.19	37.55	32.99	35.74	32.23	25.77	23.44	24.72	24.54	23.27
Cu	0.52	0.57	0.64	0.66	bdl	0.53	bdl	3.70	bdl	bdl	bdl	bdl
Total	99.99	99.79	100.00	100.00	100.01	100.00	99.99	100.00	100.01	100.99	100.06	100.00
Fe/Ni	1.8	2.1	1.3	0.7	0.7	0.8	0.8	1.4	1.8	1.7	1.7	1.8

Pn= pentlandite; mss= monosulphide solid solution